CALCULATION OF ACCEPTANCE AND EFFICIENCY FOR $D^0 \to e^+e^-$ AND RATES OF PIONS AND KAONS FAKING ELECTRON SIGNALS AT CDF

by

DALJIT K. DHALIWAL

THESIS

Submitted to the Graduate School

of Wayne State University,

Detroit, Michigan

in partial fulfillment of the requirements

for the degree of

MASTER OF SCIENCE

2006

_____

Advisor Date

I thank my advisor, Dr. Robert Harr, for guiding this research and for his continuous encouragement and support. I am grateful to Dr. Paul Karchin for his helpful suggestions and discussions. I would like to thank Edmund Berry and Ivan K. Furic from University of Chicago, Ch. Paus and Alberto Belloni from MIT , Vivek Tiwari from Carnegie Mellon Univ. and Saverio D'Auria for helping me with their unique and insightful way of approaching problems. I'd also like to thank Alfredo Gutierrez for his help, my colleague Nagesh Kulkarni for his helpful suggestions in computing. I am grateful to my parents for their encouragement. Last but not least I thank my husband for his continued support all through my Master's degree.

Contents

List of Figures

List of Tables

Chapter 1

Standard Model

1.1 Introduction

In the 19^{th} century, the fundamental units of matter were believed to be atoms. Further experiments in the the early 20^{th} century demonstrated that protons and neutrons are just two examples of a class of particles called hadrons, and that hadrons are composed of quarks bound together by gluons. This has evolved to today's Standard Model of particle physics (SM) which encapsulates our knowledge of elementary particles and the fundamental forces between them.

1.2 The Standard Model

The Standard Model consists of the subatomic particles that build up matter and the rules for their interactions using quantum theory. The strong interactions are described by quantum chromodynamics or QCD, while the weak and electromagnetic interactions are described by the electroweak theory. The gravitational interactions, though considered one of the fundamental interactions, are generally too small to play a role in particle interactions, and are omitted from the Standard Model of particle physics [1].

1.2.1 Elementary Particles

The elementary particles of the SM come in two types: spin one-half fermions and spin one bosons. The fermions are divided into leptons and quarks, and obey Fermi-Dirac statistics. The bosons are the force carriers and obey Bose-Einstein statistics. Because the interactions support gauge symmetries, the force carriers are commonly called gauge bosons.

There are six leptons and six quarks, each organized into three generations of doublets. The three charged leptons are electron(e), muon (μ) and tauon (τ). All three are associated with a neutral particle called neutrino. The three neutrinos are: electron neutrino (ν_e), muon neutrino (ν_μ) and tau neutrino (ν_τ). The six quark flavors are up (u), down (d), charm (c), strange (s), top (t) and bottom (b) quarks. Corresponding to each quark, there is an anti-quark with opposite charge. Figure 1.1 shows the Standard Model for

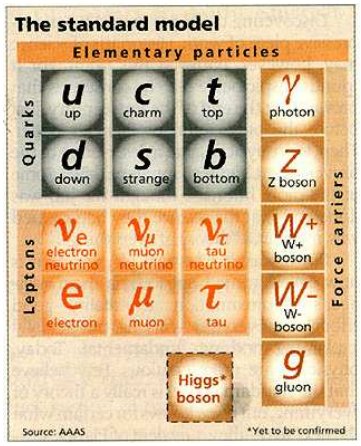

Figure 1.1: Elementary Particles and their force carriers in the Standard Model

elementary particles, showing particle generations and their force carriers. Lepton doublets are :

$$\begin{pmatrix} \nu_e \\ e \end{pmatrix} \qquad \begin{pmatrix} \nu_\mu \\ \mu \end{pmatrix} \qquad \begin{pmatrix} \nu_\tau \\ \tau \end{pmatrix}. \tag{1.1}$$

Quarks doublets or generations are written as :

$$\begin{pmatrix} u \\ d \end{pmatrix} \qquad \begin{pmatrix} c \\ s \end{pmatrix} \qquad \begin{pmatrix} t \\ b \end{pmatrix}. \tag{1.2}$$

Leptons carry integral charge values: -e , 0 , +e. Charged leptons interact through weak and electromagnetic forces and neutrinos interact via only weak forces. Masses of neutral leptons are very small or zero. Table 1.1[2] shows the measured masses or limits of the leptons.

Table 1.1: The measured masses or mass upper-limits for the leptons. Evidence for nonzero neutrino mass has been found from the observation of neutrino oscillations.

Particle	**Q**	**Mass**
e	-1	.511 MeV/c^2
μ	-1	105.65 MeV/c^2
τ	-1	1777.03 MeV/c^2
ν_e	0	< 3 eV/c^2
ν_μ	0	< 0.19 MeV/c^2
ν_τ	0	< 18.2 MeV/c^2

Table 1.2: Quark charges and their approximate masses. Quarks are spin-1/2 hadrons and carry baryon number 1/3 while anti-quarks have baryon number -1/3.

Name	**Symbol**	**Q**	**Mass**
Down	d	-1/3	350 MeV/c^2
Up	u	2/3	350 MeV/c^2
Strange	s	-1/3	550 MeV/c^2
Charmed	c	2/3	1800 MeV/c^2
Bottom	b	-1/3	4500 MeV/c^2
Top	t	2/3	175,000 MeV/c^2

Quarks interact by strong, weak and electromagnetic forces. The presence of the same flavor of quarks in a particle leads to the violation of Pauli's exclusion principle according to which no two identical fermions can occupy the same quantum state. This problem was solved by assigning an additional quantum number to quarks. This additional degree of freedom is called "color". Each quark can have one of three different colors, red, blue and green, and their anti-quarks come in the corresponding anti-colors. Table 1.2 [3] lists the charges and approximate masses of the quarks. Quarks are not

directly observable. They are found in bound states called hadrons. Hadrons are colorless objects and are formed from three quarks (or three anti-quarks) each of different color, or from a quark and anti-quark pair of a color and anti-color. Three-quark states are called baryons, and quark–anti-quark states are called mesons. Quark combinations for hadrons are:

Baryon = $Q_iQ_jQ_k$ (three quarks)

Meson = $Q_i\overline{Q_j}$ (quark-antiquark pair)

The D^0 meson consists of a charm quark and up anti-quark ($c\overline{u}$)

1.2.2 Particle Interactions

Particle interactions are mediated by the exchange of gauge bosons. The gauge bosons are spin-1 particles and follow the group structure $SU(3)_C \otimes SU(2)_L \otimes U(1)_Y$, where "C" refers to the color, "L" is lefthanded and "Y" is the weak hypercharge. The virtual photon is responsible for the electromagnetic force. Weak interactions take place with the exchange of W^+, W^- and Z^0 gauge bosons. Since the exchange of $W^\pm$ causes a change in charge they are called "charged-current" reactions while Z^0 causes no change in the charge and hence their interactions are called "neutral-current" reactions. Strong interactions take place through gluons. The gravitons which are the exchange particles for gravitational force have not been observed so far. Gluons are considered bi-colored exchange particles responsible for the color force between quarks. They are electrically neutral.

These interactions follow conservation rules [4]. They conserve momen-

tum, angular momentum, charge and CPT (charge, parity and time reversal). For strong and electromagnetic interactions C, P and T are separately conserved while weak interactions conserve none of them separately, only the total combination CPT.

1.3 Decay Modes

Decay modes are grouped by their short distance structure. Flavor changing neutral current decays (FCNC) are highly suppressed decays in the Standard Model. The FCNC decays require both the electromagnetic or strong as well as the weak interactions to occur [5]. Moreover, short distance contributions to charm decays are small, and they give an opportunity to study higher order interactions of suppressed decays in SM. Rare charm decays include processes such as $D^0 \to \mu^-\mu^+$, $D^0 \to e^-e^+$, $D^0 \to e^\pm\mu^\mp$. Table 1.3 [6] displays some of the FCNC decay modes of D mesons, along with the experimental limits on their branching fractions.

1.4 Motivation for studying charm decays

One objective for studying the heavy quarks is to address the SM predictions for FCNC transitions of charm mesons. Rare charm decays are sensitive to the effects of beyond the SM physics and hence have the potential to probe new physics. The expected short-range SM contribution for FCNC decays is

Table 1.3: The experimental limits for $D^+ \to \pi$ll, $D_s^+ \to \pi$ll, $D^0 \to l^+l^-$

Mode	**Experimental Limit**
$D^+ \to \pi^+\mu^+\mu^-$	8.8×10^{-6}
$D^+ \to \pi^+e^+e^-$	5.2×10^{-5}
$D^+ \to \pi^+\mu^\pm e^\mp$	3.4×10^{-5}
$D^+ \to \pi^-\mu^+\mu^+$	4.8×10^{-6}
$D^+ \to \pi^-e^+e^+$	9.6×10^{-5}
$D^+ \to \pi^-\mu^+e^+$	5.0×10^{-5}
$D_s^+ \to \pi^+\mu^+\mu^-$	1.4×10^{-4}
$D_s^+ \to \pi^+\mu^+\mu^-$	1.4×10^{-4}
$D_s^+ \to \pi^+e^+e^-$	2.7×10^{-4}
$D_s^+ \to \pi^+\mu^\pm e^\mp$	6.1×10^{-4}
$D_s^+ \to \pi^-\mu^+\mu^+$	8.2×10^{-5}
$D_s^+ \to \pi^+e^+e^+$	6.9×10^{-4}
$D_s^+ \to \pi^-\mu^+e^+$	7.3×10^{-4}
$D^0 \to \mu^+\mu^-$	1.3×10^{-6}
$D^0 \to e^+e^-$	1.2×10^{-6}
$D^0 \to \mu^\pm e^\mp$	8.1×10^{-7}

small due to the GIM (Glashow-Iliopoulos-Maiani) mechanism; these decays are dominated by long range effects [7]. The long range branching fraction prediction is affected by hadronic uncertainties which arise from the transition of hadrons from initial to final state. The decay $D^0 \to e^-e^+$ is a FCNC process which does not violate any standard model conservation laws but is CKM, GIM and helicity suppressed [8]. The FCNC transitions also involve the coupling of the quark flavor changing vertex to the charged current , $W^\pm$ bosons, giving rise to weak interactions. Hence, the study of such decay modes helps in the understanding of long distance effects and can be used to set an upper limit on these contributions.

The $D^0 \to e^+e^-$ branching ratio limit is determined using the following

inequality [10]:

$$\mathcal{B}(D^0 \to e^+e^-) \leq \mathcal{B}(D^0 \to K\pi)\frac{N(ee)}{N(K\pi)} \times \frac{\epsilon(K\pi)}{\epsilon(ee)} \times \frac{a(K\pi)}{a(ee)} \tag{1.3}$$

where $B(D^0 \to K^-\pi^+)$ is the normalization branching fraction, $N(ee)$ and $N(K\pi)$ are the numbers of $D^0 \to e^+e^-$ and $D^0 \to K^-\pi^+$ events observed after background subtraction, and ϵ and a are the efficiency and acceptance for each decay mode. We use Monte Carlo simulation to estimate the most significant part of the acceptance and efficiency for $D^0 \to e^+e^-$ in order to estimate the sensitivity for this decay in the data. The sensitivity is also affected by backgrounds that fake the e^+e^- final state. To estimate background from hadrons faking electrons, we used D^* tagged $D^0 \to K^-\pi^+$ decays to determine the electron fake rates for the $\pi's$ and $K's$.

Chapter 2

CDF Detector

2.1 Overview

The Collider Detector at Fermilab (CDF) is designed to study $p\overline{p}$ collisions at the Fermilab Tevatron collider. Currently, it is the world's highest energy collider, colliding beams of protons and antiprotons with energies close to 2 TeV. Studying the particle interactions at such high energies allows us to observe some rare decays and processes. Luminosity, the measure of the rate of particle collisions, is directly related to the intensity of the particle beams. It is used to calculate the event rate. The initial goal of Run II was to achieve an integrated luminosity of 2 fb^{-1} and initial luminosity of 5 $\times 10^{32} cm^{-2} s^{-1}$. There are 10^{10} - 10^{14} particles in the beam and about 500,000 $p\overline{p}$ interactions occur every second. Events are reconstructed after the particle collisions and are characterized in terms of energy and type of particles produced.

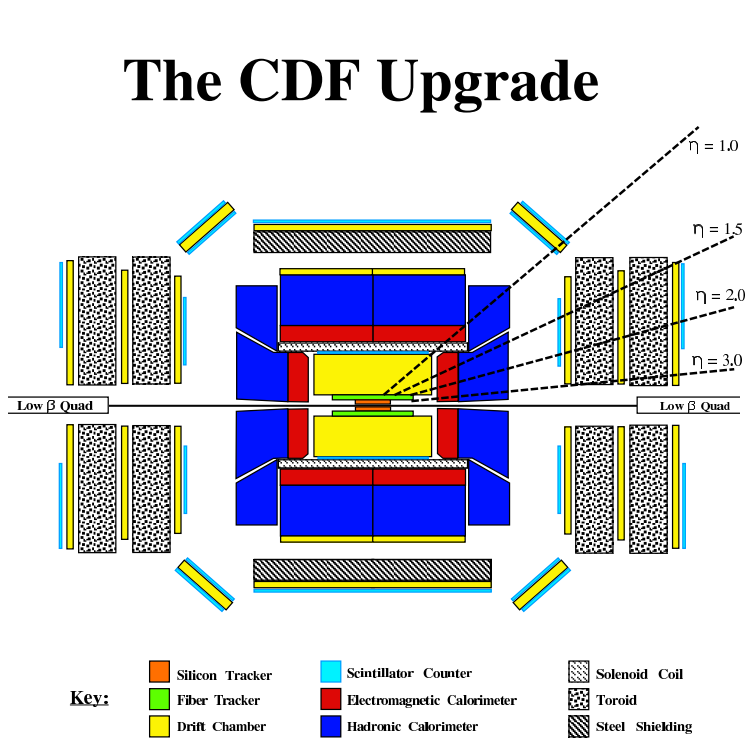

Figure 2.1: Sideview of the collider detector at Fermilab (CDF).Beams of $p\overline{p}$ collide at a center of mass energy of 2.0 TeV. The pseudorapidity coverage of various components is also shown. Source:CDF

This chapter briefly describes the CDF II detector. Figure 2.1 [11] shows an overview of the detector and Figure 2.2 shows a cutaway of the detector.

The CDF detector is a combination of individual detector elements each having complementary purposes and capabilities. The information gathered from all of them is used to analyze events. In the CDF collider experiment, the $p\bar{p}$ beams cross every 396 ns, and the trigger and data acquisition systems must be capable of handling the resulting flow of information from the detector. The detector components used in this analysis are discussed below.

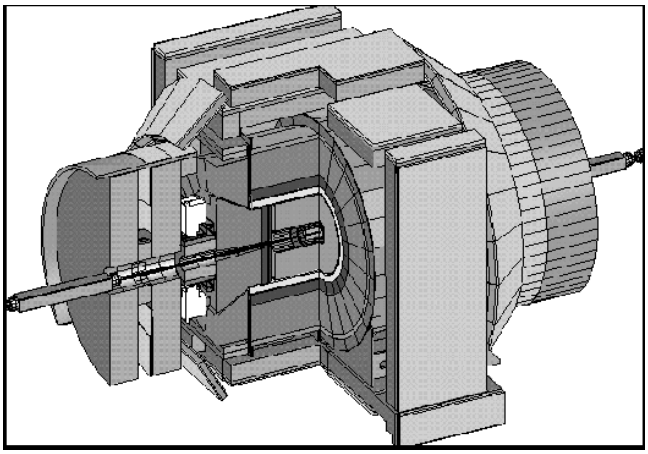

Figure 2.2: Schematic view of CDF detector with one quarter cut away to show the interior elements. Source:CDF

2.2 Tracking Detectors

2.2.1 Silicon Vertex Detector

Closest to the interaction point is the silicon vertex detector, used to accurately reconstruct production and decay vertices. The SVX II has five double sided layers of AC coupled micro-strip sensors [12] arranged symmetrically around the beampipe. Each sensor has axial strips on one side and, either stereo strips at small angles or strips at 90° on the other side. The 12-fold symmetric azimuthal geometry of the assembly makes each 30° wedge an independent tracker. Table 2.1 [13] lists some of the features of SVX II. It is sensitive to particles with pseudorapidity $|\eta| \leq 1$, where η = -ln tan $\theta/2$ and θ is the angle of the particle with respect to the proton beam. The silicon detector reconstructs particle trajectories close to the collision point and the

Table 2.1: Features of Silicon Vertex Tracker (SVX II)

SVX II	
Readout coordinates	$r-\phi$;r-z
Number of barrels	3
Number of layers per barrel	5
Number of wedges per barrel	12
Ladder length	29.0 cm
Combined barrel length	87.0 cm
Radius of innermost layer	2.44 cm
Radius of outermost layer	10.6 cm
Total number of detectors	720
Total number of ladders	180
Total number of readout chips	3168
Number of channels	405,504

secondary vertices resulting from particle decays.

2.2.2 Central Outer Tracker

Outside the silicon detector is the central outer tracker. The tracking detectors are immersed in a 2T magnetic field parallel to the colliding beams. The momentum of charged particles are measured by the curvature of their trajectories in the magnetic field. The trajectories are determined from measurements of the drift time of the ionized electrons in the gas. The energy loss per unit length (dE/dx) is found from the charge collected due to ionization. The energy loss is proportional to the velocity of the particle, and when combined with the measured momentum, allows the particle mass to be calculated. Track dE/dx measurements are used in the electron identification algorithm discussed in Chapter 4. Table 2.2 [11] lists some of the

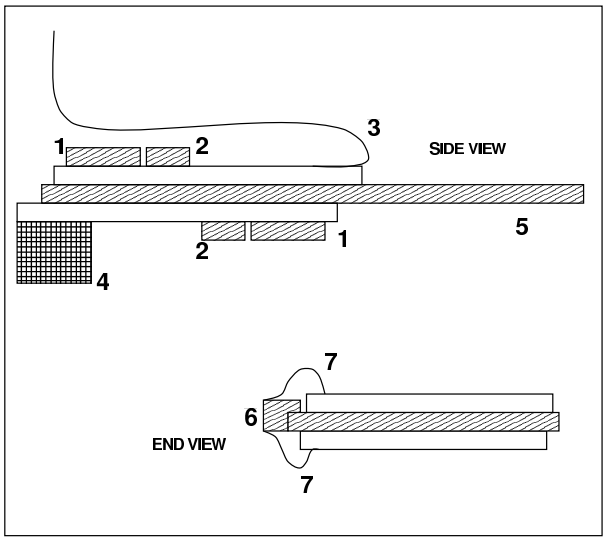

Figure 2.3: Silicon Vertex Detector(SVX) accurately detects the path of the particle by measuring initial and azimuthal directions. Source: CDF SVX II webpage

features of the COT at CDF.

Table 2.2: Features of the Central Outer Tracker(COT)

COT	
Number of superlayers	8
Measurements per superlayer	12
Radius at the center	46 58 70 82 94 106 119 131 cm
Tilt Angle	35
Length of active region	310cm
Number of channels	30,240

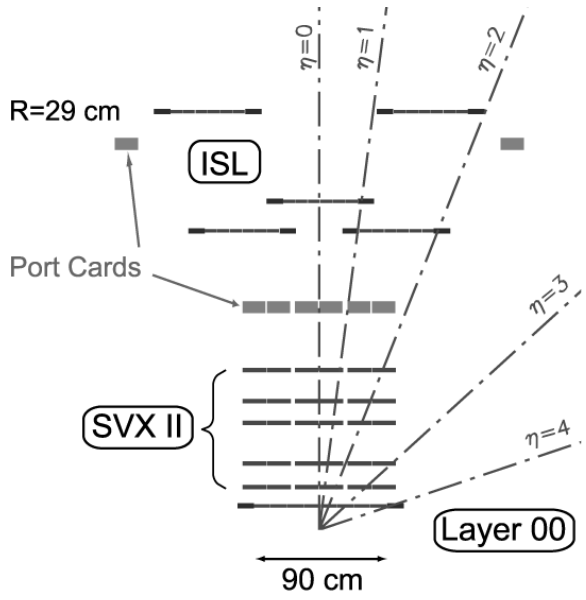

Figure 2.4: Cross section of silicon vertex tracker of the CDF Run II. Source: CDF

2.3 Time-of-Flight System

The time-of-flight (TOF) system consists of scintillator bars located outside the COT and readout by photomultiplier tubes at each end. It is designed to distinguish low transverse momentum kaons from pions. Information about time-of-flight is included in the electron identification algorithm discussed in Chapter 4. By measuring the time required to traverse some specific distance in the detector, the speed of the particle can be inferred. The momentum of the particle measured by the COT along with the speed measured by TOF is combined to determine the mass of the particle. The time resolution of the detector limits the mass resolution in CDF. The time-of-flight resolution

potential is 100 ps. This is sufficient to distinguish kaons from pions for momenta up to 1.6 GeV/c.

2.4 Solenoid

The CDF tracking system and TOF are located inside a superconducting solenoidal magnet generating a field of 2 T. It operates at liquid helium temperature and is able to support currents up to 5000 A. The track curvature in the magnetic field enables the transverse momentum of charged particles to be measured with a precision of $\frac{\delta P_T}{P_T} = (0.002/GeV)P_T$.

2.5 Calorimeters

The calorimeter is divided into two parts, electromagnetic and hadronic calorimeters. The electromagnetic calorimeters are designed to measure the energy of electrons and photons [14], and are used in this analysis to identify electrons. Table 2.3 lists details of the calorimeter segmentation.

Table 2.3: CDF II Calorimeter Segmentation

$\lvert\eta\rvert$	$\Delta\Phi$	$\Delta\eta$
0 - 1.1	15°	0.1
1.1 - 1.8	7.5°	0.1
1.8 - 2.1	7.5°	0.16
2.1 - 3.64	15°	0.2 - 0.6

2.6 Data Acquisition and Trigger system

In CDF, event selection is made with a three level trigger system. How data flows through the trigger and data acquisition system is shown in Fig 2.5 [15].

Level-1 uses custom hardware and processes about 1.7 million crossings/sec. It reduces the data rate from the bunch crossing frequency of 1.7 MHz to 30 kHz. Level-2 also uses custom hardware and selects about 1000 events/sec. Level-3 uses a farm of Linux PC's and selects about 400 events/sec which are then stored for later analysis offline. Fig 2.6 shows a block diagram of data flow in the CDF data acquisition network. Fig 2.7 shows a block diagram of the three level pipelined and buffered trigger system at CDF. The CDF data acquisition (DAQ) consists of front end VMS crates, time-to-digital converters and trigger cards.

Data is buffered at the frontend crate during level 1 and level 2 trigger processing. Data passing level-2 is collected from the front end, organized by the event builder, and sent to the level-3 farm. After the level-3 trigger accepts an event, data is written to permanent storage tape.

2.6.1 Level-1

This analysis relies on data collected with the two-track trigger (TTT). This completely track-based trigger is designed to select events containing heavy quark decays. The XFT (extremely Fast Tracker) is a part of level-1 trigger

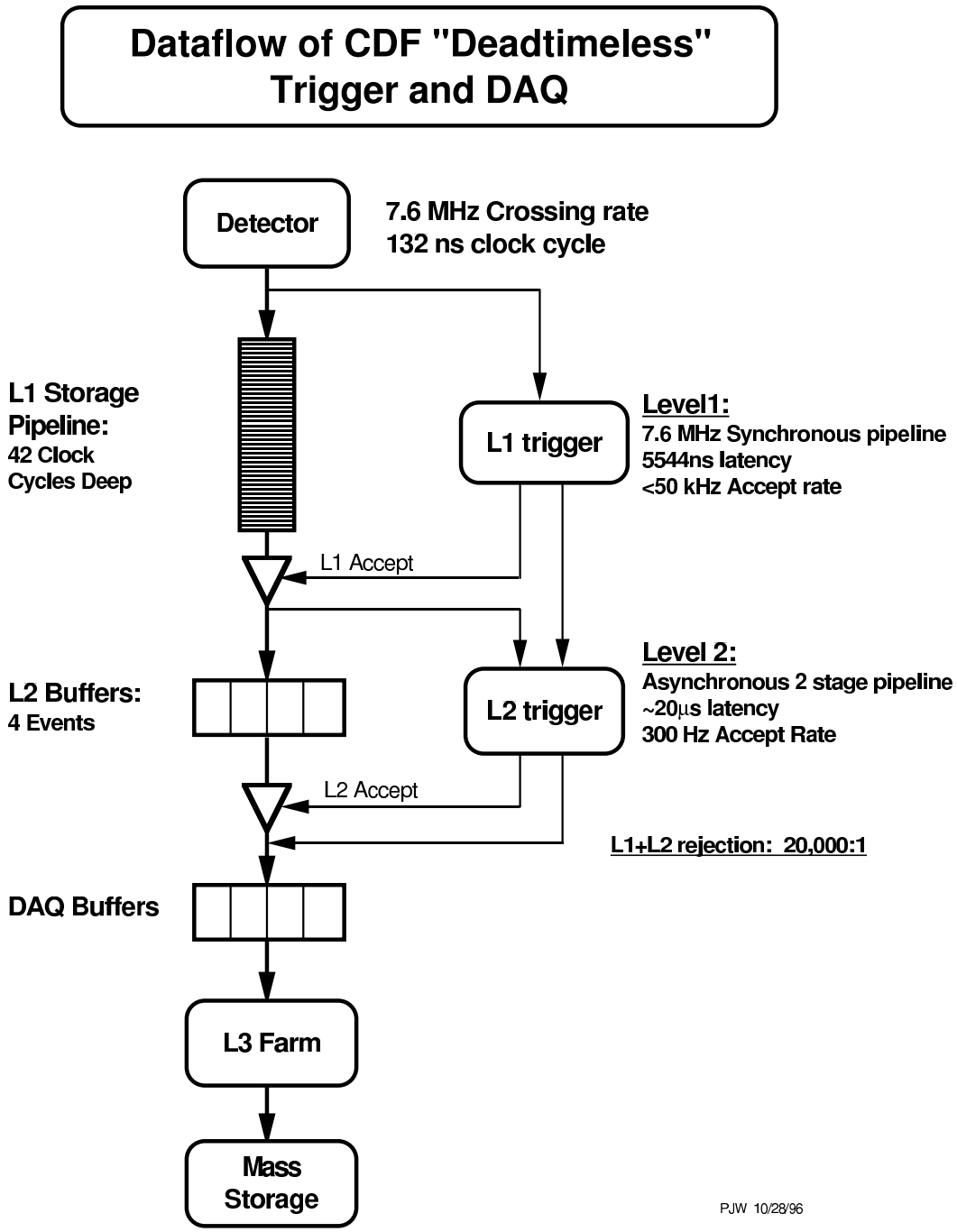

Figure 2.5: Dataflow of CDF dead-timeless trigger and DAQ. Source: CDF DAQ system

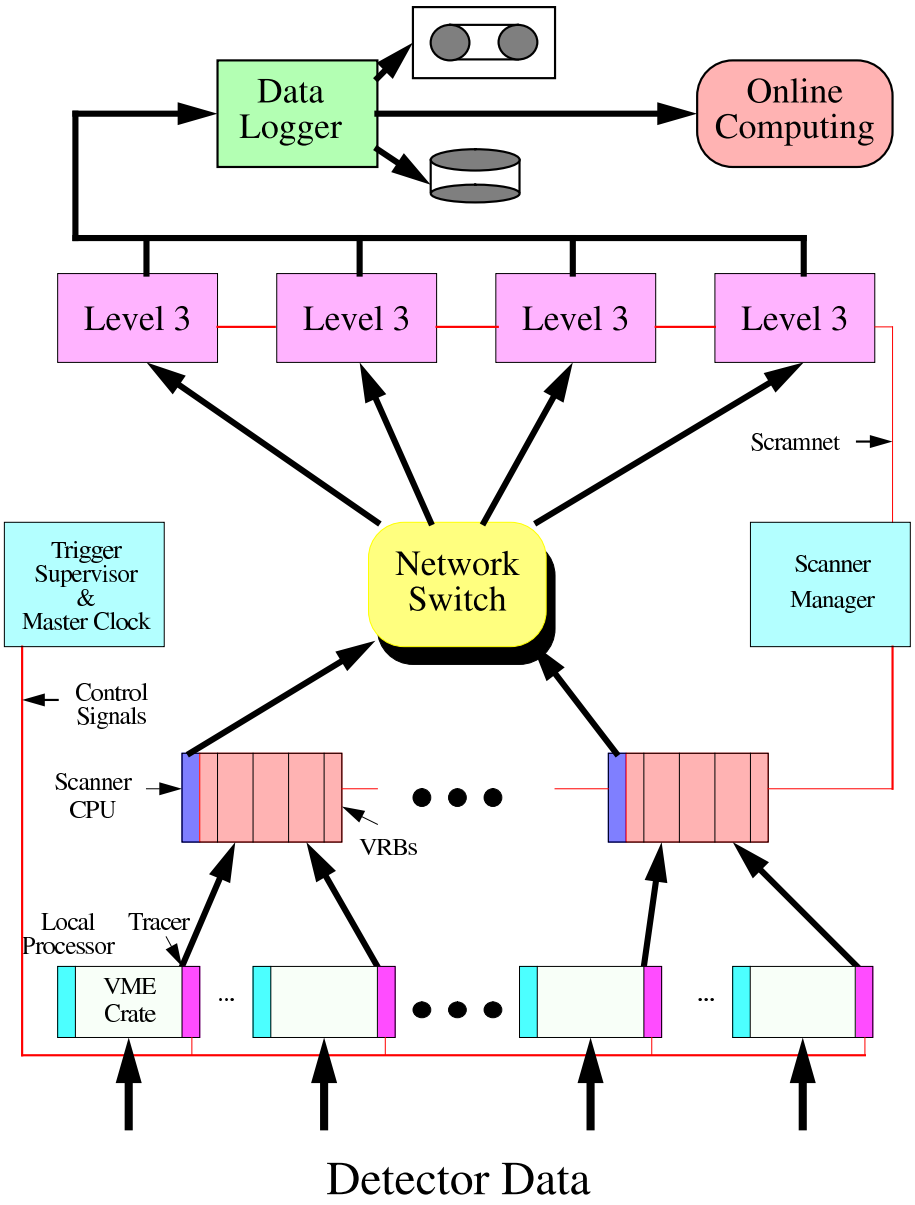

Figure 2.6: Block diagram of the data flow of the CDF data acquisition (DAQ) network. Source:CDF

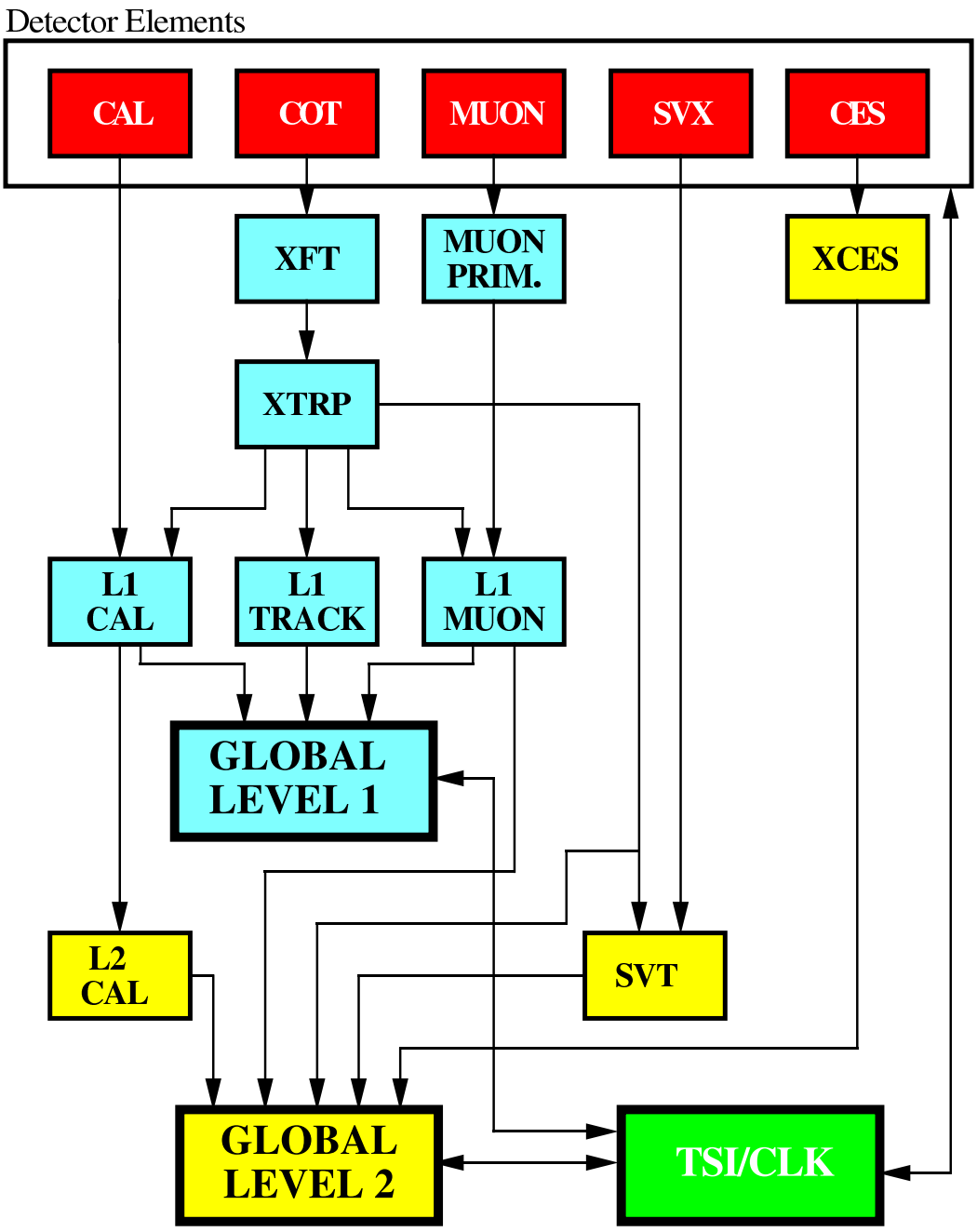

Figure 2.7: Block diagram of the first two levels of the trigger system at CDF. Source:CDF

system and finds tracks with transverse momentum $P_T > 1.5 GeV/c$. The XFT reconstructs tracks by finding line segments in the four axial superlayers and linking them into tracks. The line segment consists of hits on 11 (sometimes 10) of 12 wires in a superlayer. Events with two XFT tracks of $P_T > 2.0 GeV/c$, $P_{T1} + P_{T2} > 5.5 GeV/c$, oppositely charged, and with an opening angle between 2° and 135° are selected for further processing.

2.6.2 Level-2

Level-2 receives events passing the level-1 trigger. The two track trigger (TTT) selects events enriched in heavy flavors based on observing effects of the small displacement of hadrons containing heavy flavors. This is accomplished with the silicon vertex tracker (SVT). The SVT adds SVX hits to the XFT tracks and measures their impact parameters. The selection at this level requires:

- 2 SVT tracks with opposite charge and $P_T \geq 2 GeV/c$,
- $2° < |\Delta\phi| < 90°$, where $\Delta\phi$ is the opening angle between the two tracks,
- scalar sum of transverse momenta, $P_{T1} + P_{T2} \geq 5.5 GeV/c$
- $120\mu m \leq |d_{SVT}| \leq 1mm$, where d_{SVT} is the impact parameter in the x-y plane with respect to the average beam position,

- the two tracks have to form a vertex which is separated from the primary vertex by 200 μm to 1 mm.

2.6.3 Level-3 and Data Acquisition

For the TTT, level-3 does no additional selection, but performs full event reconstruction. The reconstructed events are written to tape for later offline analysis.

Chapter 3

Monte Carlo Simulation

3.1 Introduction

Monte Carlo (MC) techniques use pseudo-random number generation for the simulation of stochastic processes. We used this technique for the simulation of production, decay, and detector response of D^* tagged D^0 decays. We generate D^*s with the `BGEN` package, according to a measured p_T distribution, decay the D^*s and D^0s with the `EVTGEN` program, and simulate the detector response with `GEANT` [16]. Full event simulation has following steps:

- event generation,
- event pre-selection,
- simulation of detector response,
- simulation of trigger and event selection, and

- full event reconstruction.

3.1.1 Event Generation

To generate Monte Carlo events, we follow the instructions for B-Physics Monte Carlo using software release 5.3.4[17] [See Appendix B]. CdfSim is the main simulation executable which uses different generators to generate events. To study specific decays, selections are made for the initial state particles and their p_T distribution. For this analysis, the events were generated using `BGen` to study the D^* tagged D^0 decay. Particle decay is simulated using the `EvtGen` decay package with a decay table containing just the modes $D^{*+} \rightarrow D^0\pi^+$, and $D^0 \rightarrow e^+e^-$ or $D^0 \rightarrow K^-\pi^+$ (and their charge conjugates). The decay tables used for generating $D^0 \rightarrow K^-\pi^+$ and $D^0 \rightarrow e^+e^-$ decays are reproduced in Appendix A. Running the `makeplan.pl` script builds the tcl files with all the instructions for program execution. The run list covering run numbers from 138809 to 186598 was used for the datasets. This created a directory containing a list of jobs, simulation, and trigger simulation tcl files. To generate Monte Carlo events for larger set of files, jobs can also be run on the central analysis farm (CAF). CAF is a large linux based farm of computers used to run batch analysis jobs [18].

3.1.2 Event Pre-Selection

All possible D^* tagged D^0 decays are filtered at this level. The selection cuts set up the filters to reject decays that have an exceedingly small probability to satisfy the trigger requirements. The two pre-selection cuts at this level require the D^0 daughter particle satisfy :

- $p_{T1} + p_{T2} \geq 4.0$ GeV/c, where p_{T1} and p_{T2} are the momentum for two particle tracks with opposite charge.

- $0.015 < \Delta\Phi < 1.8$ radians, $\Delta\Phi$ is the opening angle.

3.1.3 Simulation of detector response

CDF uses the `GEANT` 3.15 package for detector simulation [16]. It is configured for the detector geometry; characteristics of the detector such as magnetic field, voltage, detector misalignments, dead regions, calibrated beam position, and detector resolutions used for simulation of events are supplied [19]. Each sub-detector is simulated to describe its actual response in terms of energy deposits, run conditions, and particle interactions with the detector materials. This ensures that events generated by Monte Carlo simulation are similar to the ones observed by the CDF detector. The detector simulation produces "fake" raw data consisting of tracking chamber hits, calorimeter and TOF signals, and stored in the same format as real data. Additionally, information about the generated particles is stored for later offline use.

3.1.4 Simulation of trigger and event selection

The response of the two-track trigger is simulated by passing the raw detector signals through a trigger simulation algorithm. At level-1, the algorithm finds tracks with $P_T > 1.5$ GeV/c from the hits in the axial COT layers, simulating the XFT. At level-2, the algorithm starts with the XFT tracks with $P_T > 2$ GeV/c, finds SVX hits that match to form SVT tracks, and selects pairs of the SVT tracks that satisfy the level-2 requirements of Sec. 2.6.2.

3.1.5 Full event reconstruction

The simulated data are passed to the CDF event reconstruction software. In the end, production is run on these events. The generated output is saved and further analyzed. Fig 3.1 shows the reconstruction of a simulated event.

`CandsExe` is then run on the Monte Carlo generated events in the same manner that it is run on real data, discussed in Chapter 4. `CandsExe`, a BStntuple maker, finds the D^* tagged decays of $D^0 \to K^-\pi^+$ and $D^0 \to e^+e^-$. The selection criteria applied to the D^* and D^0 decays are summarized in Table 3.1.

The tcl file used to run `CandsExe` has information on the decay chain of the particles, their tracks etc. The module used for collection of the particles tagging D^0 is included in its tcl file.

All the D* candidates for which these decay modes are not found are dropped. The `TStnMaker` module writes the selected events in the Stntuple

Table 3.1: Selection cuts applied to the D^* and D^0 decays.

	selection cuts
Trigger pair	K π or ee
Impact parameter	must be of opposite sign for both trigger pairs.
Decay Length	$200\mu m \leq L_{xy}(D^0) \leq 1200\mu m$
Impact Parameter	$\|\Delta z_0\| \leq 5cm$
Min. and Max. mass	$1.50GeV/c^2 - 2.00GeV/c^2$
Maximum value of χ^2	$\chi^2 < 15$

[20]. This procedure selects 8978 and 5914 events for $D^0 \rightarrow K^-\pi^+$ and $D^0 \rightarrow e^+e^-$ decay modes respectively. The BStntuple so formed is further analyzed.

An executable is built which is run on the BStntuples. The header file in the executable `TCandsntuples.hh` defines the method and the data members. `TCandsntuples.cc` contains the code for each method defined in its header file. The `runntuples` script defines the particles and their id's in the decay and creates the analysis framework. Setting up the analysis module, it adds data blocks to it. The output is written in the form of a root tree in which selected event information is stored. This step selects 7328 $D^0 \rightarrow K^-\pi^+$ candidates and 1860 $D^0 \rightarrow e^+e^-$ events. It is still unclear which selection requirement causes the steep drop from 5914 to 1860 in the number of $D^0 \rightarrow e^+e^-$ events. This can be looked at to improve the efficiency and acceptance value.

3.2 Acceptance and Efficiency

The Monte Carlo simulation is used to find the acceptance and relative efficiency of $D^0 \rightarrow e^+e^-$ and $D^0 \rightarrow K^-\pi^+$ decay. The number of events recorded by the detector are reduced by the acceptance and efficiency. Since the coverage of the detector is not 100%, some of the events slip through the blind spots and hence are not recorded. This loss of events is due to the acceptance of the detector. Acceptance effects arising from processes like bremsstrahlung, positron interactions, and scattering are included in the Monte Carlo simulation. The ionization difference between electrons, kaons and pions is not simulated and hence this small effect on the track reconstruction efficiency is not evaluated here.

A three level trigger system selects the D^0 decays for the analysis. The Cabibbo favored $D^0 \rightarrow K^-\pi^+$ decay was chosen for the normalization and optimization of the selection criteria. The selection requirements are the same for both modes. To study the relative acceptance and efficiency for the D* tagged $D^0 \rightarrow e^+e^-$ and $D^0 \rightarrow K^-\pi^+$, we generated 100,000 events of each type. To select the $D^0 \rightarrow K^-\pi^+$ and $D^0 \rightarrow e^+e^-$ decays, the invariant mass of each pair of trigger tracks is calculated with all possible track mass assignments ($K^-\pi^+$, $K^+\pi^-$, e^+e^-). The D^0 candidates are selected in the invariant mass range $1.50GeV/c^2 < M_{inv} < 2.05GeV/c^2$.

The charge of the soft pion π_s, and the pion from D^0 decay are required to be of same sign and the mass difference ΔM = m($D^0\pi_s$) - m(D^0) should

Table 3.2: The ratio of number of entries in $D^0 \rightarrow e^+e^-$ to $D^0 \rightarrow K^-\pi^+$ decay mode. The $D^0 \rightarrow K^-\pi^+$ mass range was help constant, yielding $N_{K\pi}$ = 7328.

Mass Range (GeV/c^2)	N_{ee}	$(\boldsymbol{A} \pm \Delta A)\%$
1.845 - 1.885	250	3.41 ± 0.05
1.825 - 1.885	354	4.83 ± 0.06
1.805 - 1.885	430	5.86 ± 0.07
1.785 - 1.885	502	6.85 ± 0.09
1.765 - 1.885	558	7.61 ± 0.09
1.745 - 1.885	620	8.46 ± 0.10
1.725 - 1.885	665	9.07 ± 0.11
1.705 - 1.885	726	9.91 ± 0.12
1.685 - 1.885	781	10.66 ± 0.13

be in the range $0.144 GeV/c^2 < \Delta M < 0.147 GeV/c^2$.

To find the branching fraction for $D^0 \rightarrow e^+e^-$ decay, we need to calculate the ratio of efficiency and acceptance of the two decay modes. The number of entries in the signal region of $D^0 \rightarrow K^-\pi^+$ decay is calculated by taking the integral over mass range 1.845 GeV/c^2 to 1.885 GeV/c^2 (Fig. 3.2). To try to recover some of the statistics in the low mass tail of the e^+e^- mass spectrum, we evaluate the number of entries for $D^0 \rightarrow e^+e^-$ decay (Fig. 3.3) over the mass ranges listed in Table 3.2. Keeping the signal window for $D^0 \rightarrow K^-\pi^+$ constant, the ratio of entries for e^+e^- decays to the number of entries for $K^-\pi^+$ decays is calculated. This ratio is the product of efficiency and acceptance for the two modes.

A is the product of efficiency and acceptance :

$$A = \frac{\epsilon(ee)}{\epsilon(K\pi)} \times \frac{a(ee)}{a(K\pi)} = \frac{N_{ee}}{N_{K\pi}}. \tag{3.1}$$

The number of entries for the normalization mode $D^0 \to K^-\pi^+$ is 7328. As the mass window for the $D^0 \to e^+e^-$ is increased, A increases from $3.41 \pm 0.05\%$ to $10.66 \pm 0.13\%$. The uncertainty in A is derived using propagation of errors, assuming poissons errors on $N_{K\pi}$,

$$\Delta A = \sqrt{\frac{A(1+A)}{N_{K\pi}}} \tag{3.2}$$

where A is the product of acceptance and efficiency and $N_{K\pi}$ is the number of entries in $D^0 \to K\pi$ decay.

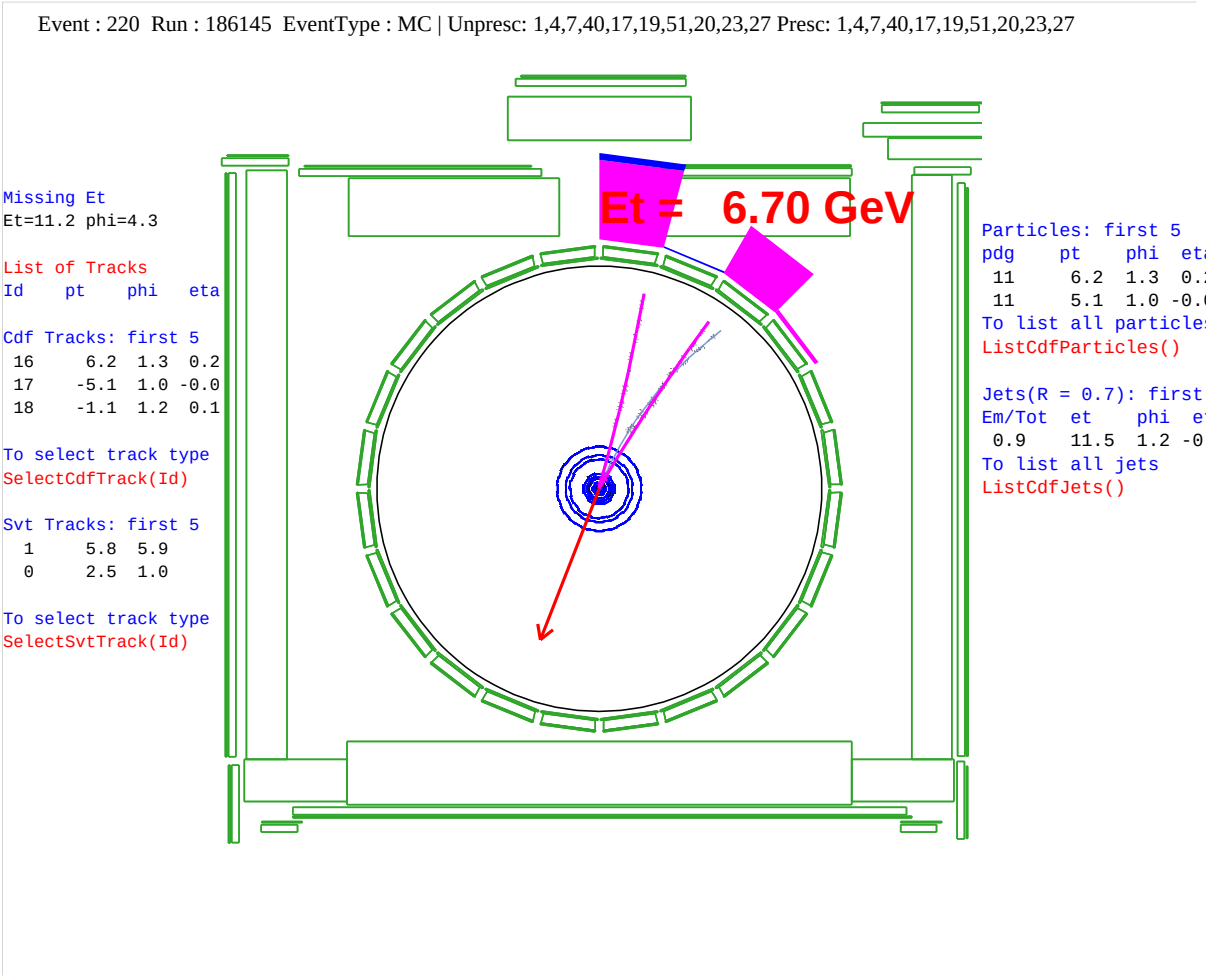

Figure 3.1: Reconstruction of a simulated event in the CDF detector. The reconstructed tracks from a D^* decay appear in the COT. The shaded trapezoids represent energy deposits in the calorimeters

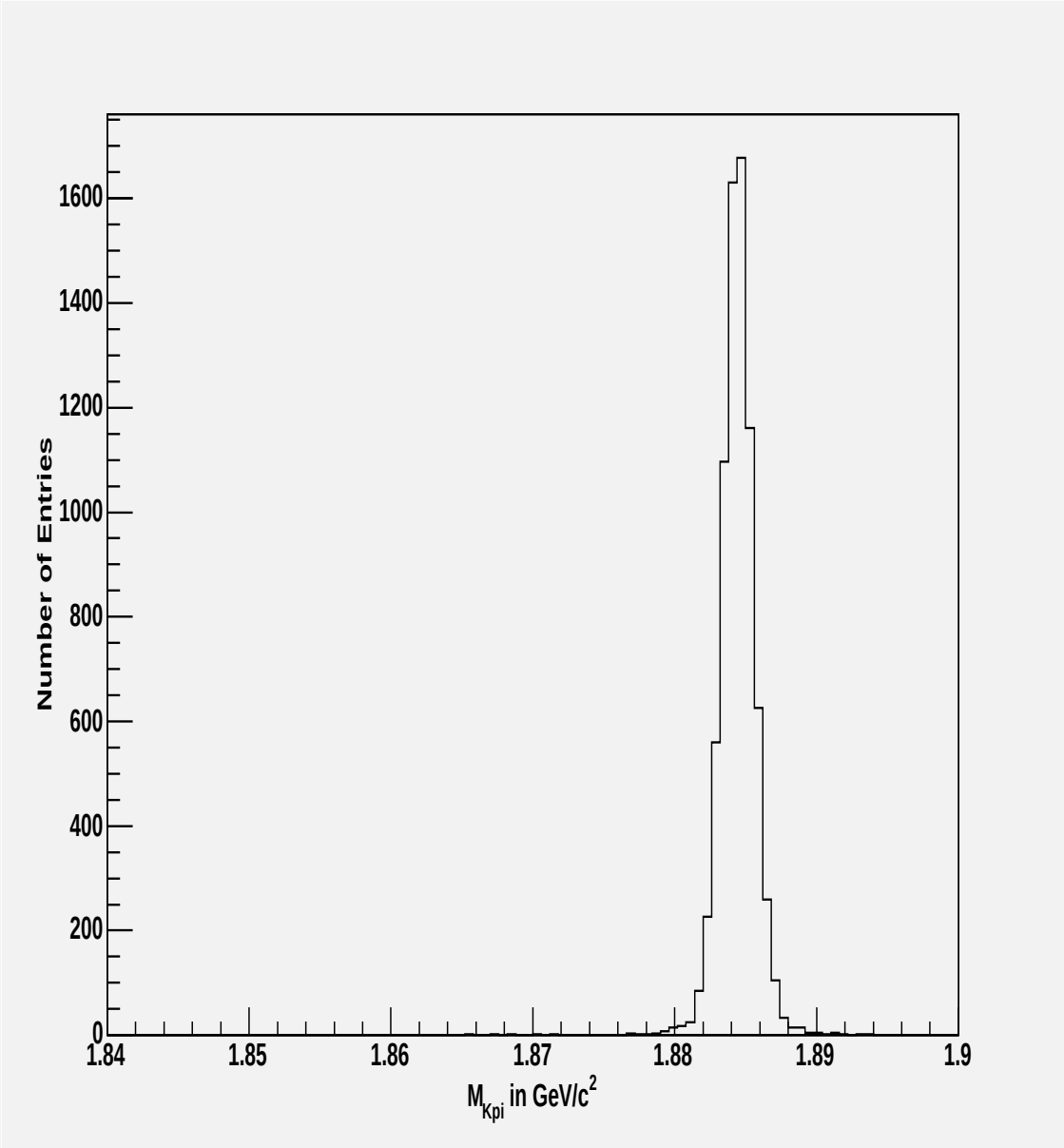

Figure 3.2: The invariant mass distribution for D* tagged $D^0 \rightarrow K^-\pi^+$ decay mode from the Monte Carlo sample. The signal window is defined as the range $1.845 GeV/c^2 < M_{K\pi} < 1.885 GeV/c^2$.

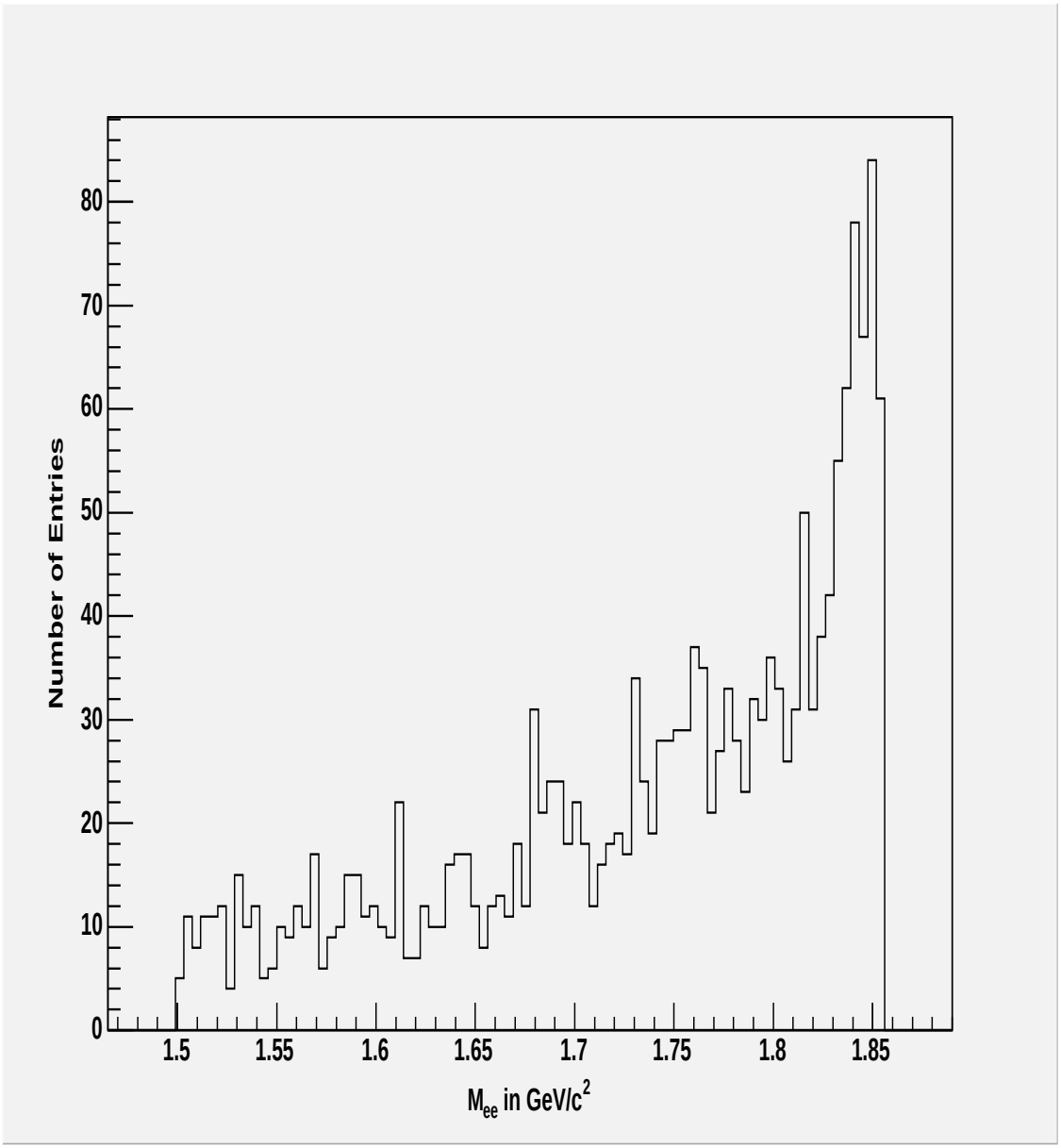

Figure 3.3: The invariant mass spectrum for $D^0 \rightarrow e^- e^+$ decay from the Monte Carlo sample. Final state radiation and bremsstrahlung produce the low mass tail. The signal window is varied as given in Table 3.2.

Chapter 4

Data Sample and Analysis

A BStntuple called h77jc0 was made from the hbot0d and hbot0h datasets by the MIT group. We use this dataset to investigate the rates of pions and kaons faking electrons. These data were reconstructed with CDFSOFT version 5.3.4, but stored in a way that requires version 6.1.1 software to read. The data sample contains about 2.6 $\times 10^8$ events out of which 1.2 $\times 10^8$ events were processed in this analysis. We create a sample of high purity K and π tracks by selecting events consistent with the $D^{*+} \rightarrow D^0 \pi_s^+$ and $D^0 \rightarrow K^- \pi^+$ decay chain (and the charge conjugate). The events are required to satisfy the following offline track quality selection criteria:

- to study the $D^0 \rightarrow K^- \pi^+$ decay, the K^- and π^+ tracks must have satisfied the two track trigger,
- the number of axial and stereo COT hits on the K, π, and π_s tracks is greater than or equal to 25,

- offline transverse momenta must satisfy $P_T > 0.5 GeV/c$ or $P_T > 2.0 GeV/c$ for trigger tracks,

- the Kπ invariant mass must lie in the range $1.50 GeV \leq m_{K\pi} \leq 2.05 GeV$, and

- the mass difference [m($K\pi\pi_s$) - m(Kπ)] must lie in the range 0.144 GeV/$c^2 \leq \triangle m \leq$ 0.147 GeV/c^2.

The same executable built for the Monte Carlo was run on this dataset and created a root tree.

Electrons are identified with a likelihood function [21] that combines information from the calorimeters, time-of-flight, and dE/dx systems. For this analysis, we use likelihood $\mathcal{L}_e > 0.9$ as the requirement for electron identification. Fake rates are derived by comparing the sideband subtracted $D^0 \rightarrow K^-\pi^+$ yields with and without the electron identification requirement applied to either the kaon or pion track. The fake rates are used to estimate backgrounds in the rare decay analysis and to get a better estimation of the sensitivity for $D^0 \rightarrow e^+e^-$ decay.

The selection cuts substantially reduce the background while only slightly reducing the signal. By tagging the soft pion from the D^* decay, the background from random combinations of tracks which accidently give the correct mass is reduced and the charge of the soft pion is used to tag the kaon and pion tracks.

About 7.3×10^5 $D^* \rightarrow D^0\pi_s^+$ and $D^0 \rightarrow K^-\pi^+$ candidates (or charge conjugates) are selected for further analysis. Information about the decays is stored in a root tree. An analysis template is used to analyze the root files. Additional quality cuts are applied at this level which further filter the events.

- We require the decay length to be positive to reduce the combinatoric background, $L_{xyz} > 0$. (see Fig. 4.4)
- We require the χ^2 on the reconstructed D^0 vertex to be $\chi^2 < 9$. (see Fig 4.5)
- The transverse momenta for pion and kaon must lie between 2.0 GeV/c and 15.0 GeV/c. (see Fig 4.2 and 4.3)
- The mass difference, Δm, between the D^* and D^0 candidates must lie between 0.144 $GeV/c^2 < \Delta m < 0.147$ GeV/c^2. (see Fig 4.1)
- To identify a track as an electron, likelihood cuts are imposed on both pion and kaon. Separate mass distributions are plotted for K^+, K^-, π^+, π^- with and without electron Id's. We use a uniform requirement of $\mathcal{L} > 0.9$, where $\mathcal{L}$ is the electron likelihood and lies between 0 and 1.

The $K\pi$ invariant mass, $M_{K\pi}$ for the decay modes $D^0 \rightarrow K^-\pi^+$ and $\overline{D^0}$ $\rightarrow K^+\pi^-$ are plotted for the range $1.7GeV/c^2 < M_{K\pi} < 2.0GeV/c^2$ in Figs 4.6 and 4.9. The mass spectrum is fitted with two Gaussian distributions and a first order polynomial, to verify the central value of the peak for the choice

of a mass window, We find the central gaussian centered at 1.865 GeV/c^2 with a width of 9 MeV/c^2. The mass spectra for each Kπ pair with the electron likelihood requirement applied to each track separately, are shown in Figs. 4.7, 4.8, 4.10 and 4.11.

The number of $D^0 \rightarrow K^-\pi^+$ signal candidates is the integral of the histogram over a $\pm 20 MeV/c^2$ mass window around 1.865 GeV/c^2. To correct for the background beneath the signal peak, we perform a sideband subtraction. The sidebands are chosen, one above and one below the signal peak, 1.785 GeV/c^2 to 1.825 GeV/c^2 for the low mass sideband, SB1, and 1.905 GeV/c^2 to 1.945 GeV/c^2 for the high mass sideband, SB2.

The electron fake rates are calculated using:

$$f_{x \rightarrow e} = \frac{(N_{sig} - N_{SB})^{\mathcal{L}>0.9}}{(N_{sig} - N_{SB})^{All}} \tag{4.1}$$

where x is one of K^+, K^-, π^+ and π^-, N_{SB} is the average of the events in the sidebands on either side of signal window, and N_{sig} is the number of events in the signal peak. The numbers of selected events in the signal region and the sidebands for the particles $K^\pm$ and $\pi^\pm$, with and without electron likelihood are displayed in Table 4.1.

Because the sidebands are of equal size, the average of the two is simply calculated by:

$$N_{SB} = \frac{N_{SB1} + N_{SB2}}{2} \tag{4.2}$$

Table 4.1: Summary of the event yields for determining the electron fake rates. The electron identification requirement $\mathcal{L} > 0.9$ is applied separately to K^-, π^+, π^-, and K^+. The number of events in the signal and sideband regions are determined from Figs 4.6 to 4.11 in $D^0 \to \mathrm{K}\pi$ decay and are used to calculate the corresponding electron fake rates.

Particle	K^-	π^+	π^-	K^+
Sideband (SB1)	7553	7553	7778	7778
Signal(sig)	227167	227167	243301	243301
Sideband(SB2)	3414	3414	3421	3421
N_{SB}	5484	5484	5600	5600
$N_{sig} - N_{SB}$	221683	221683	237701	237701
with $\mathcal{L} > 0.9$	K^-	π^+	π^-	K^+
Sideband(SB1)	49	193	205	54
Signal(sig)	170	624	524	167
Sideband(SB2)	42	47	52	44
N_{SB}	46	120	129	49
$N_{sig} - N_{SB}$	124	504	395	118
$f_{x\to e} \times 10^{+4}$	(5.59 ± 0.50)	(22.7 ± 0.98)	(16.6 ± 0.39)	(4.96 ± 0.46)

where N_{SB1} is the number of events in the low mass region and N_{SB2} is the number of events in the high mass region.

From the event yields in the $D^0 \to K^-\pi^+$ decay with and without the electron identification requirement $\mathcal{L} > 0.9$, the electron fake rates are determined. They are found to be 5.59×10^{-4} for K^-, 2.27×10^{-3} for π^+, 1.66×10^{-3} for π^- and 4.96×10^{-4} for K^+.

The uncertainty on the electron fake rate is calculated using error propagation [22] :

$$\delta f = \sqrt{\frac{N^2_{\mathcal{L}\leq 0.9}\Delta N^2_{\mathcal{L}>0.9} + N^2_{\mathcal{L}>0.9}\Delta N^2_{\mathcal{L}\leq 0.9}}{(N_{\mathcal{L}\leq 0.9} + N_{\mathcal{L}>0.9})^4}} \tag{4.3}$$

where $N_{\mathcal{L}\leq 0.9}$ is the number of entries in the signal range after background subtraction with likelihood less than equal to 0.9, $N_{\mathcal{L}>0.9}$ is the number of entries in signal range with background subtraction and with likelihood cut. $\Delta N_{\mathcal{L}\leq 0.9}$ and $\Delta N_{\mathcal{L}>0.9}$ are the respective uncertainties, assumed to be poissonian.

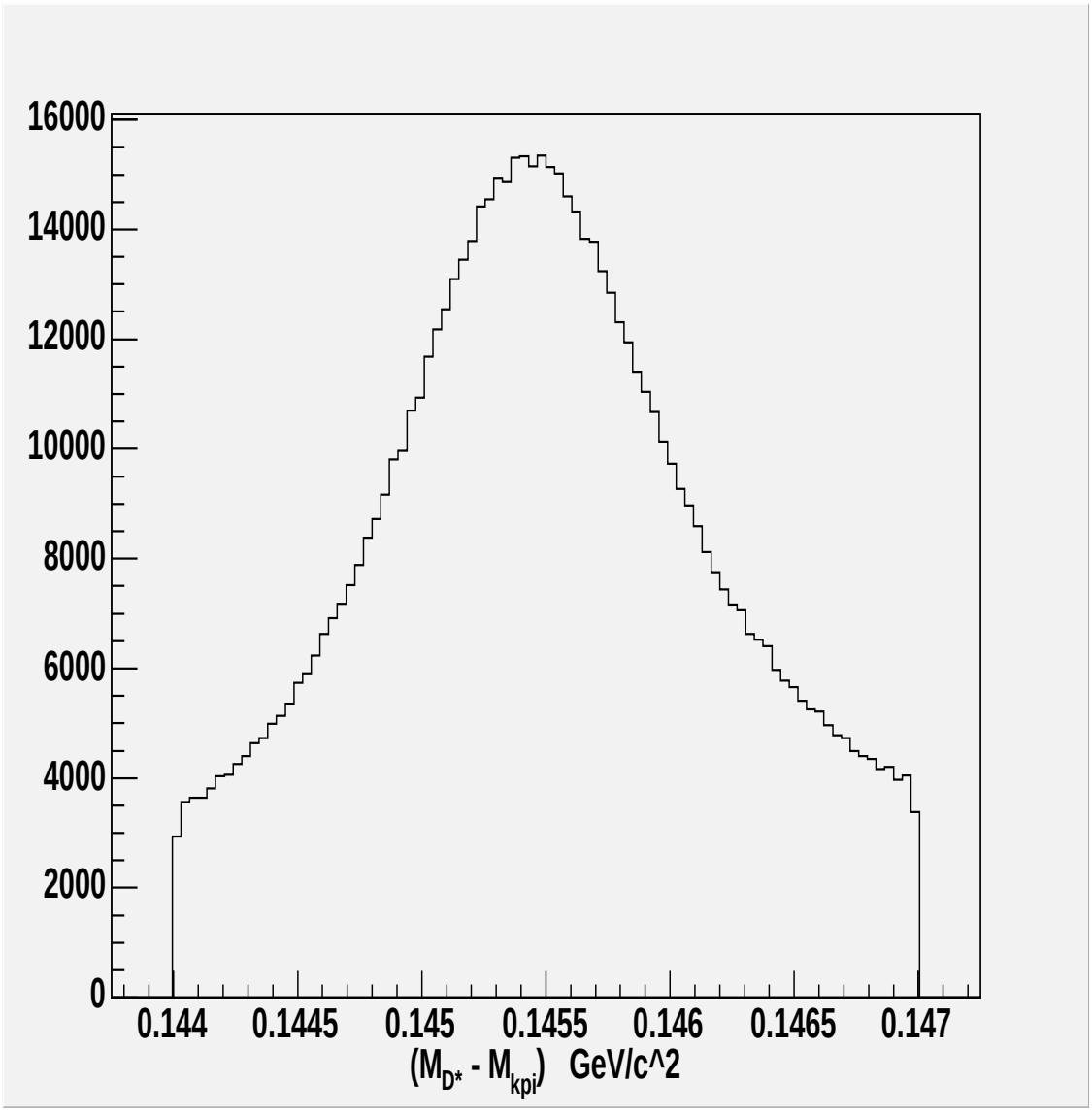

Figure 4.1: The mass difference distribution [M(D^*) - M($K\pi$)] for D^* tagged $D^0(K\pi)$ decay in the range 0.144 GeV/c^2 < mass diff < 0.147 GeV/c^2.

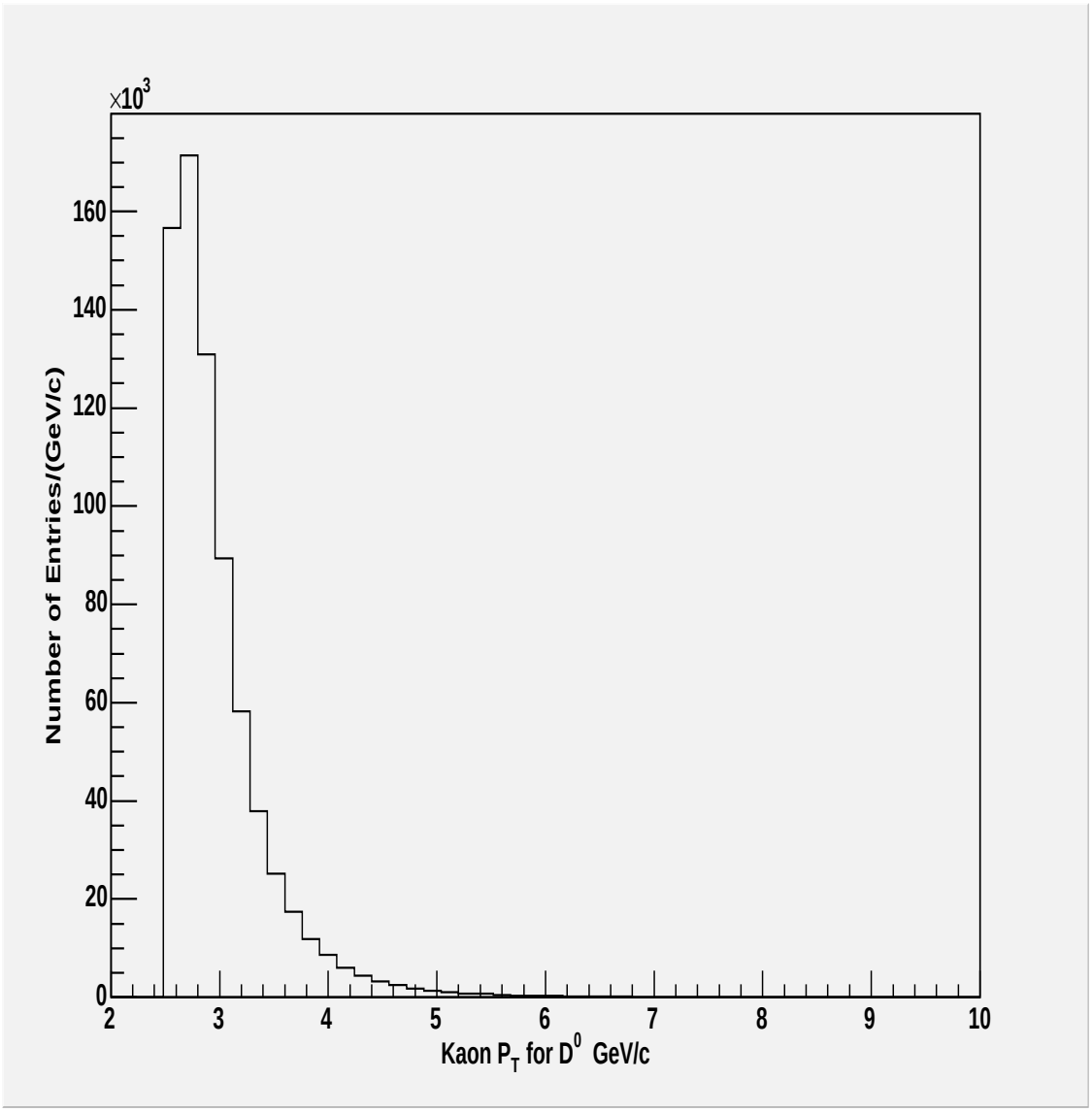

Figure 4.2: The transverse momentum distribution of the kaon for $D^0 \to K\pi$ decay.

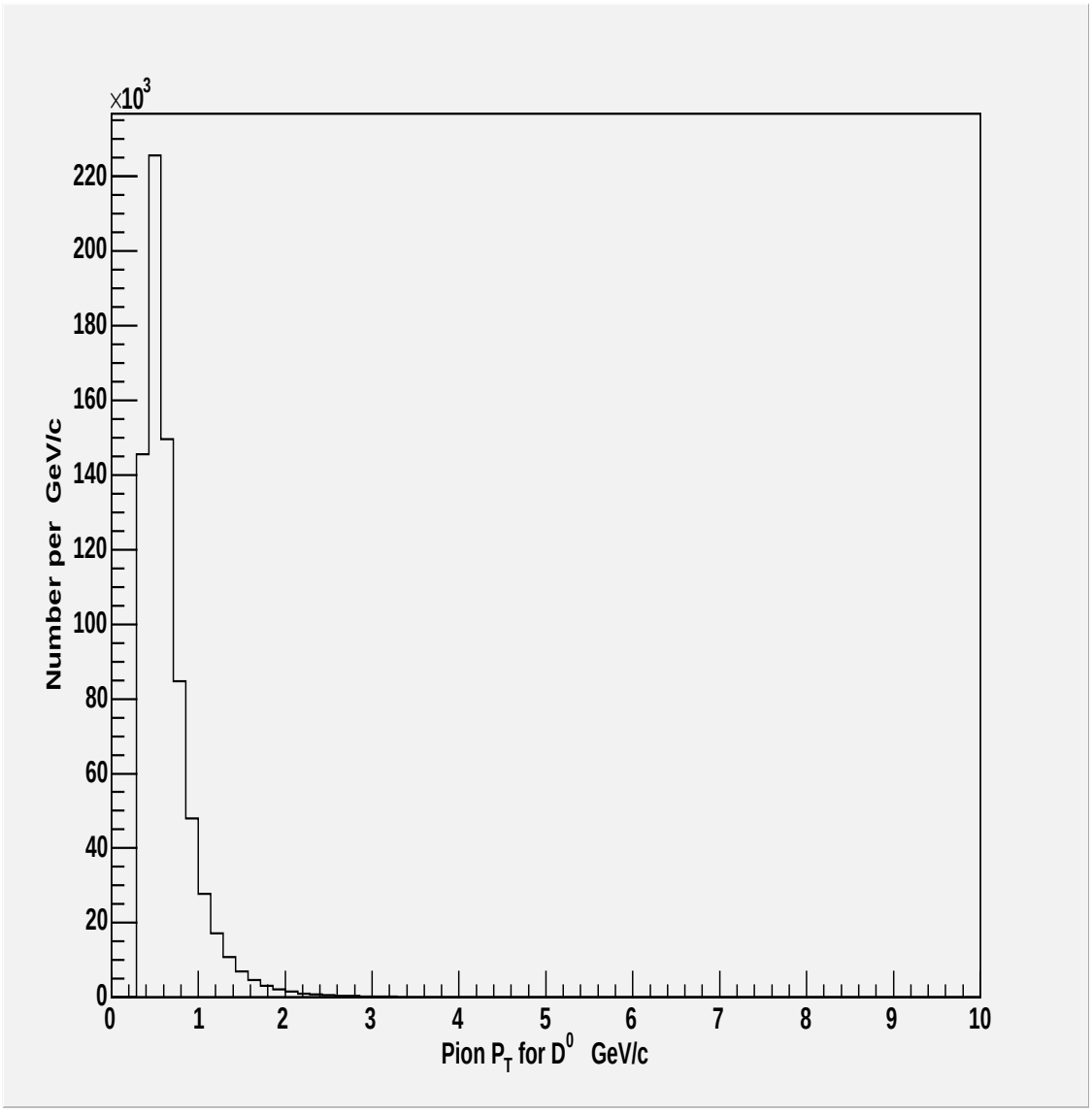

Figure 4.3: The transverse momentum distribution of the pion for $D^0 \rightarrow K\pi$ decay.

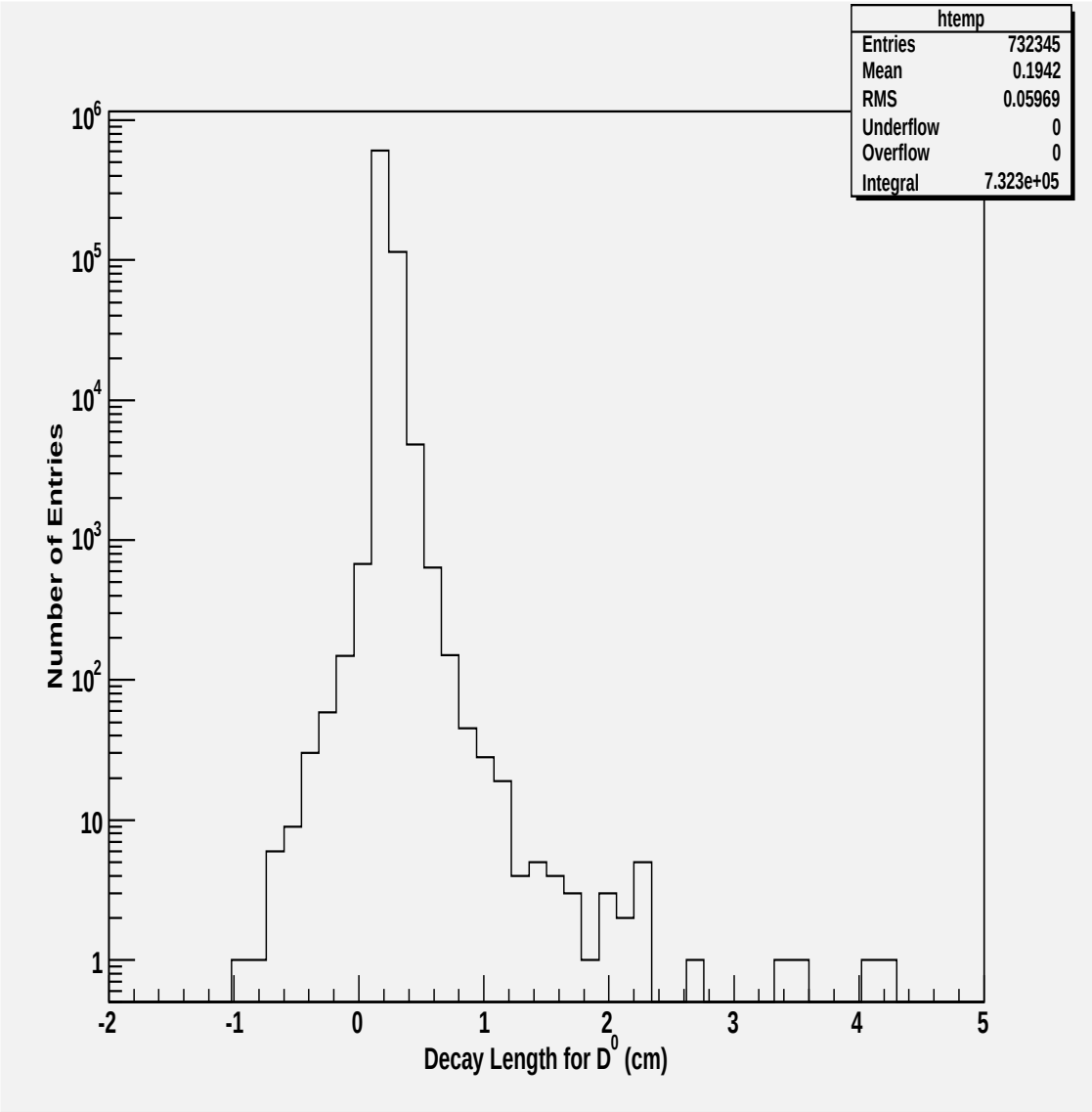

Figure 4.4: Distribution for the reconstructed decay length L_{xyz} of D^0. The cut on the decay length reduces the combinatoric background for the $D^0 \rightarrow$ Kπ decay

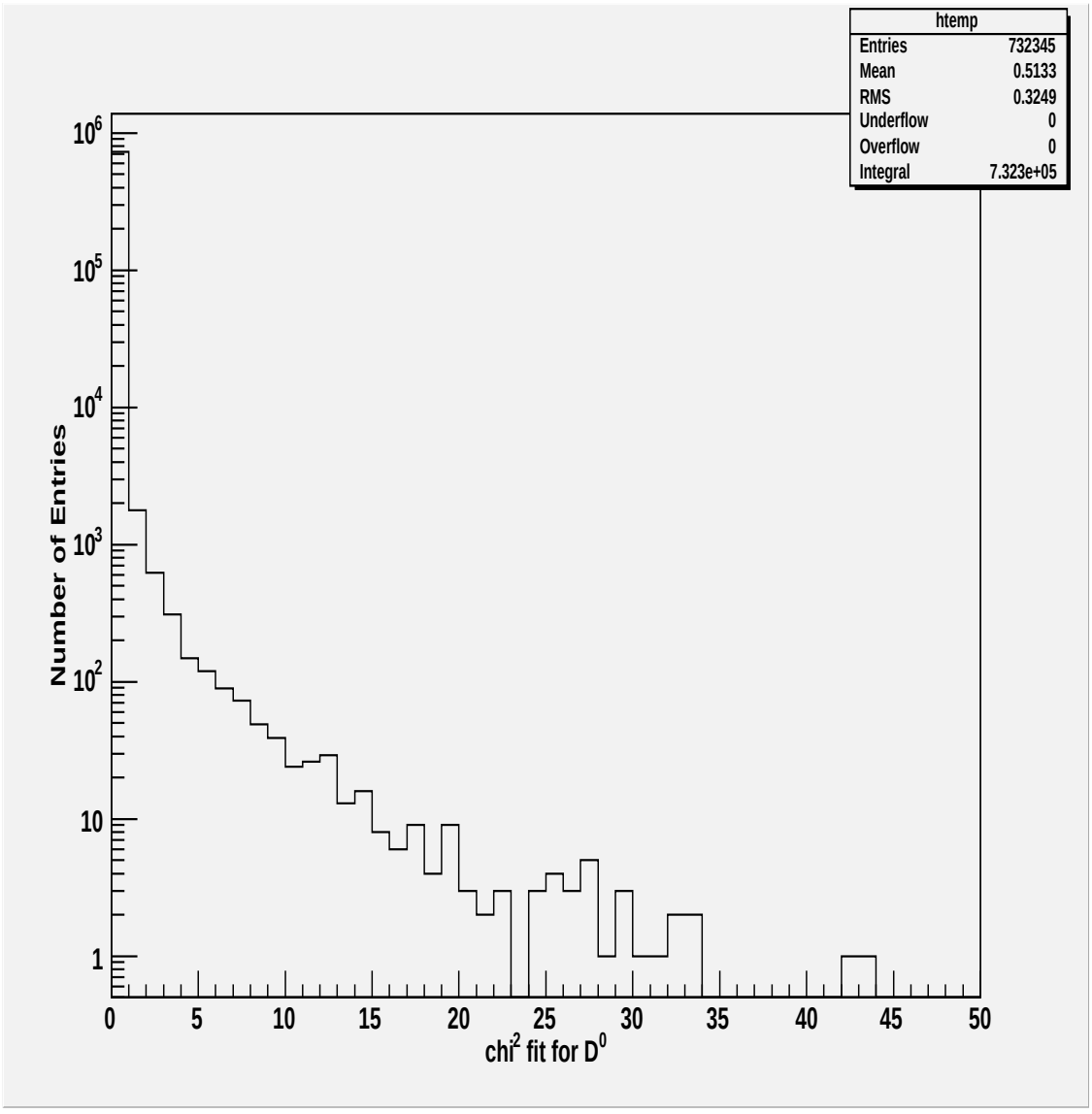

Figure 4.5: The χ^2 fit of the D^0 vertex, in the D* tagged $D^0 \to K^-\pi^+$ decay. We remove events with $\chi^2 > 9$, indicating a poor fit to a vertex.

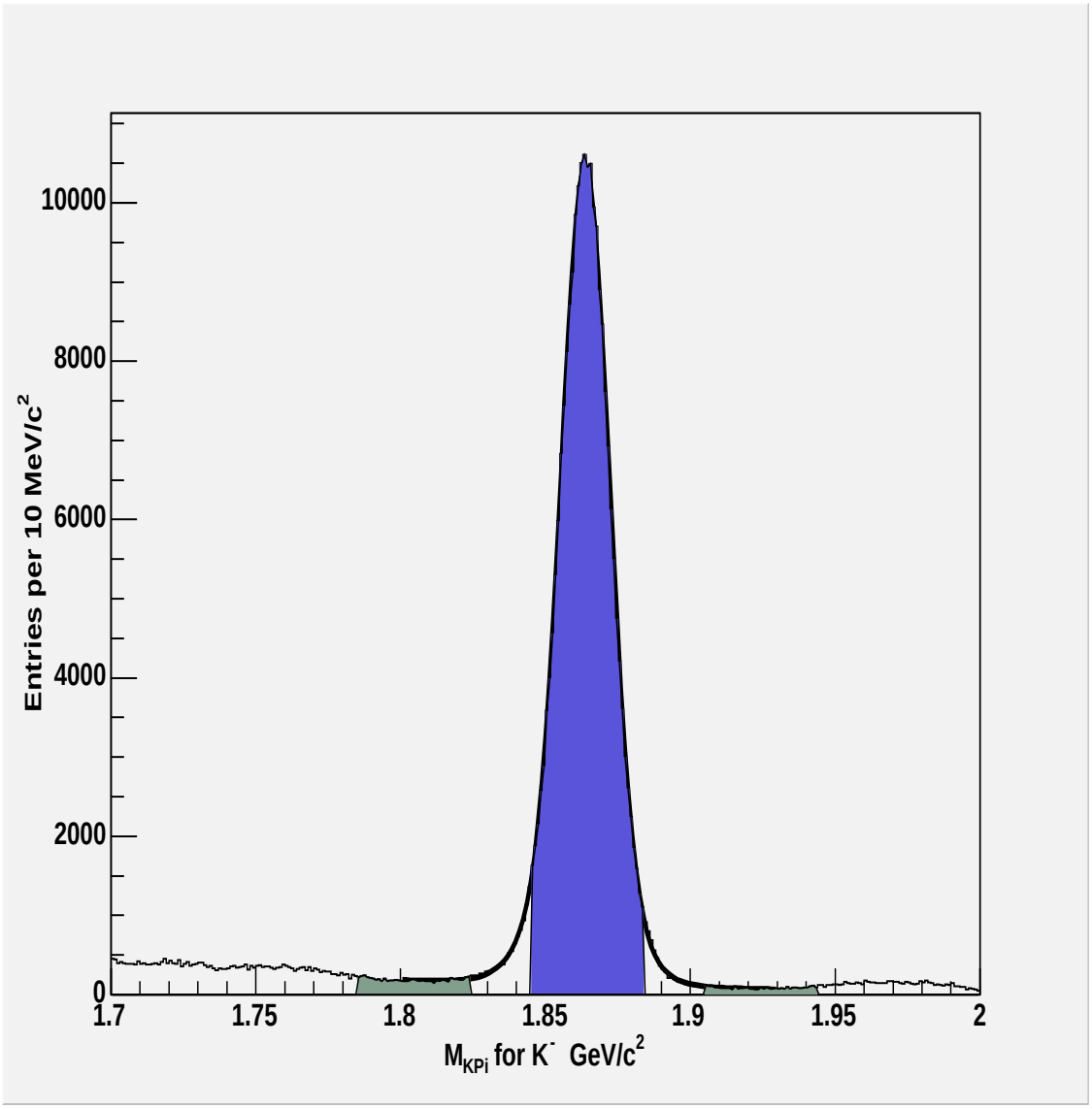

Figure 4.6: The $K^-\pi^+$ invariant mass spectrum without an electron likelihood requirement for D^* tagged $D^0 \to K^-\pi^+$ candidates. The background is fitted with two gaussian distributions and a first order polynomial. The mass window for the signal peak lies between 1.845 GeV/c^2 - 1.885 GeV/c^2. The lighter shaded regions on both sides of the signal peak are the sidebands used to estimate the background.

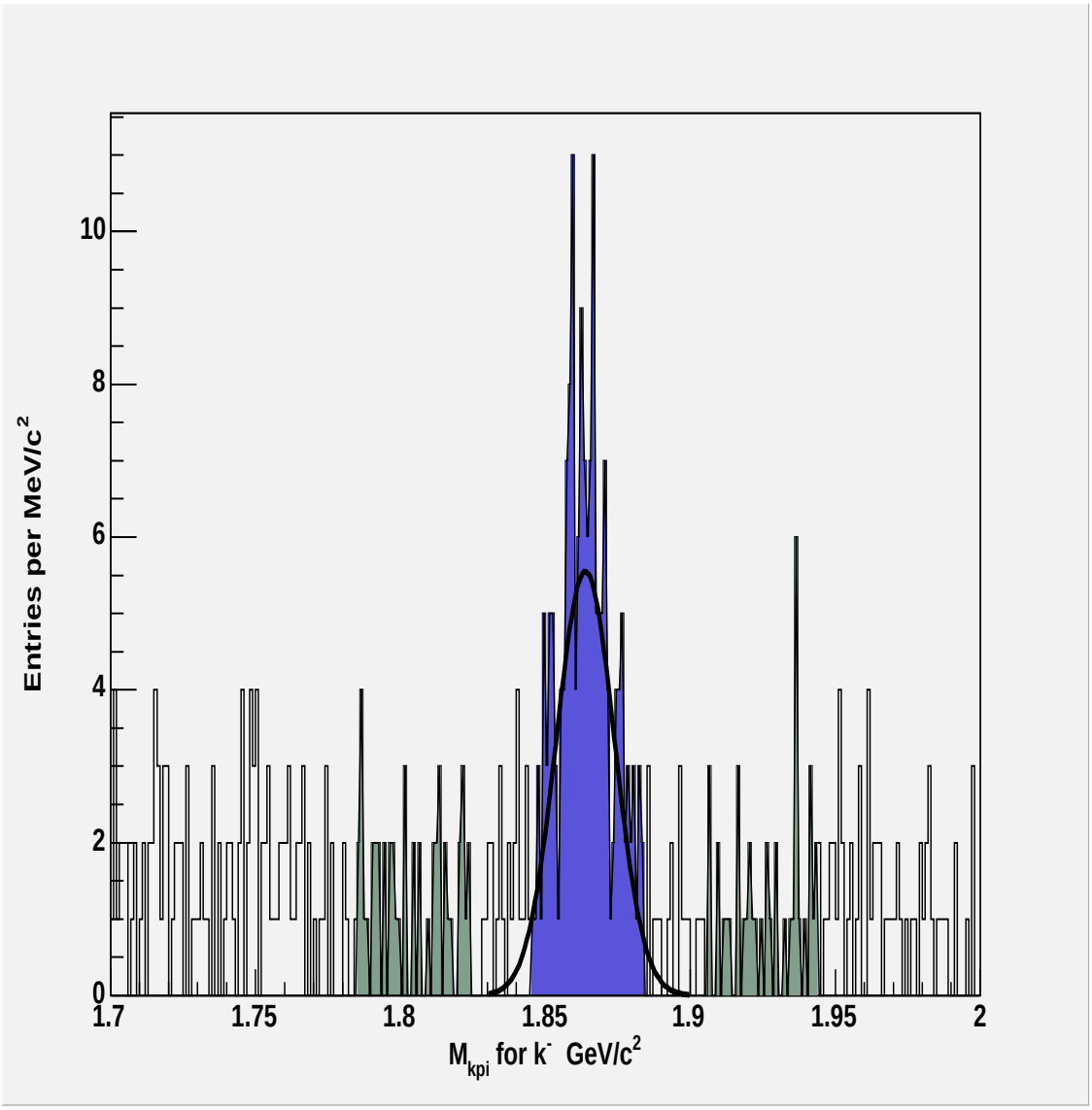

Figure 4.7: The mass distribution spectrum for the K^- particle with the electron likelihood in $D^0 \rightarrow \mathrm{K}\pi$ decay. Gaussian signal over the range 1.83 GeV/c^2 to 1.90 GeV/c^2 is fit over the signal peak. The mass window for the signal peak lies between 1.845 GeV/c^2 - 1.885 GeV/c^2.The lighter shaded regions on both sides of signal peak are the sidebands used to estimate the background.

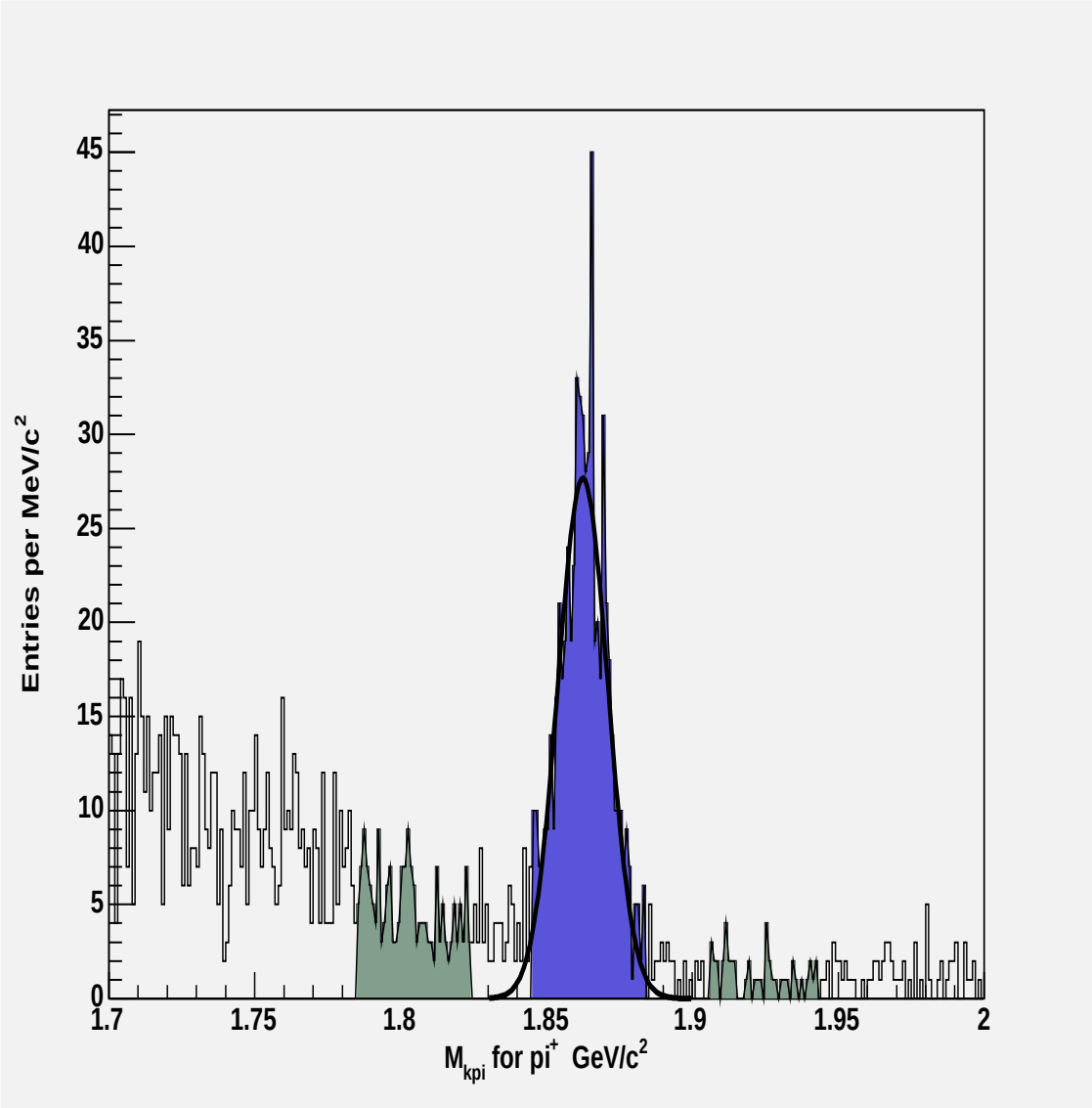

Figure 4.8: The mass distribution spectrum for the π^+ particle with the electron likelihood in $D^0 \rightarrow K\pi$ decay. Gaussian signal over the range 1.83 GeV/c^2 to 1.90 GeV/c^2 is fit over the signal peak. The mass window for the signal peak lies between 1.845 GeV/c^2 - 1.885 GeV/c^2.The lighter shaded regions on both sides of signal peak are the sidebands used to estimate the background.

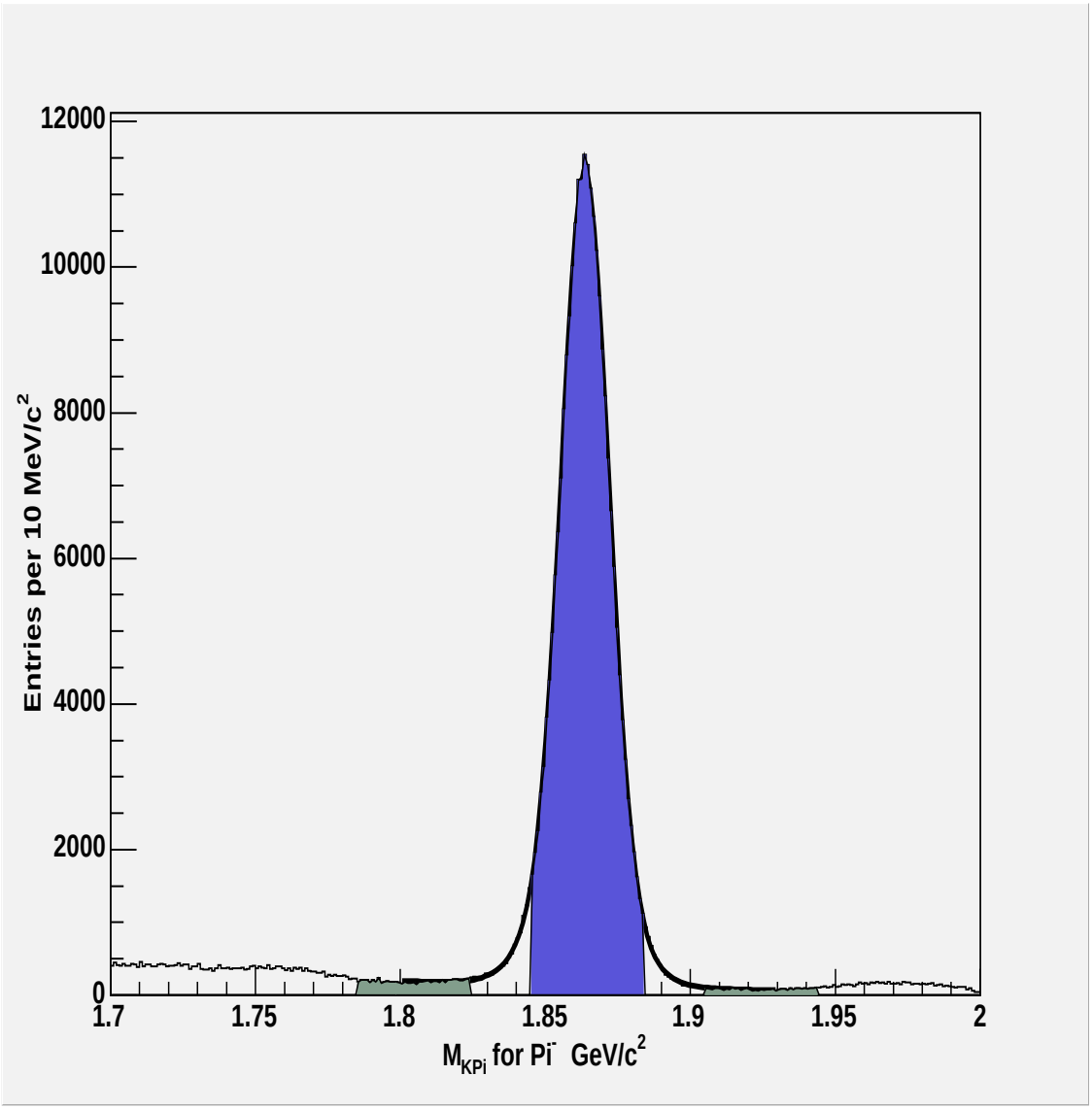

Figure 4.9: The $K^-\pi^+$ invariant mass spectrum without an electron likelihood requirement for D^* tagged $D^0 \to K^-\pi^+$ candidates. The background is fitted with two gaussian distributions and a first order polynomial. Gaussian signal over the range 1.83 GeV/c^2 to 1.90 GeV/c^2 is fit over the signal peak. The mass window for the signal peak lies between 1.845 GeV/c^2 - 1.885 GeV/c^2.The lighter shaded regions on both sides of signal peak are the sidebands used to estimate the background.

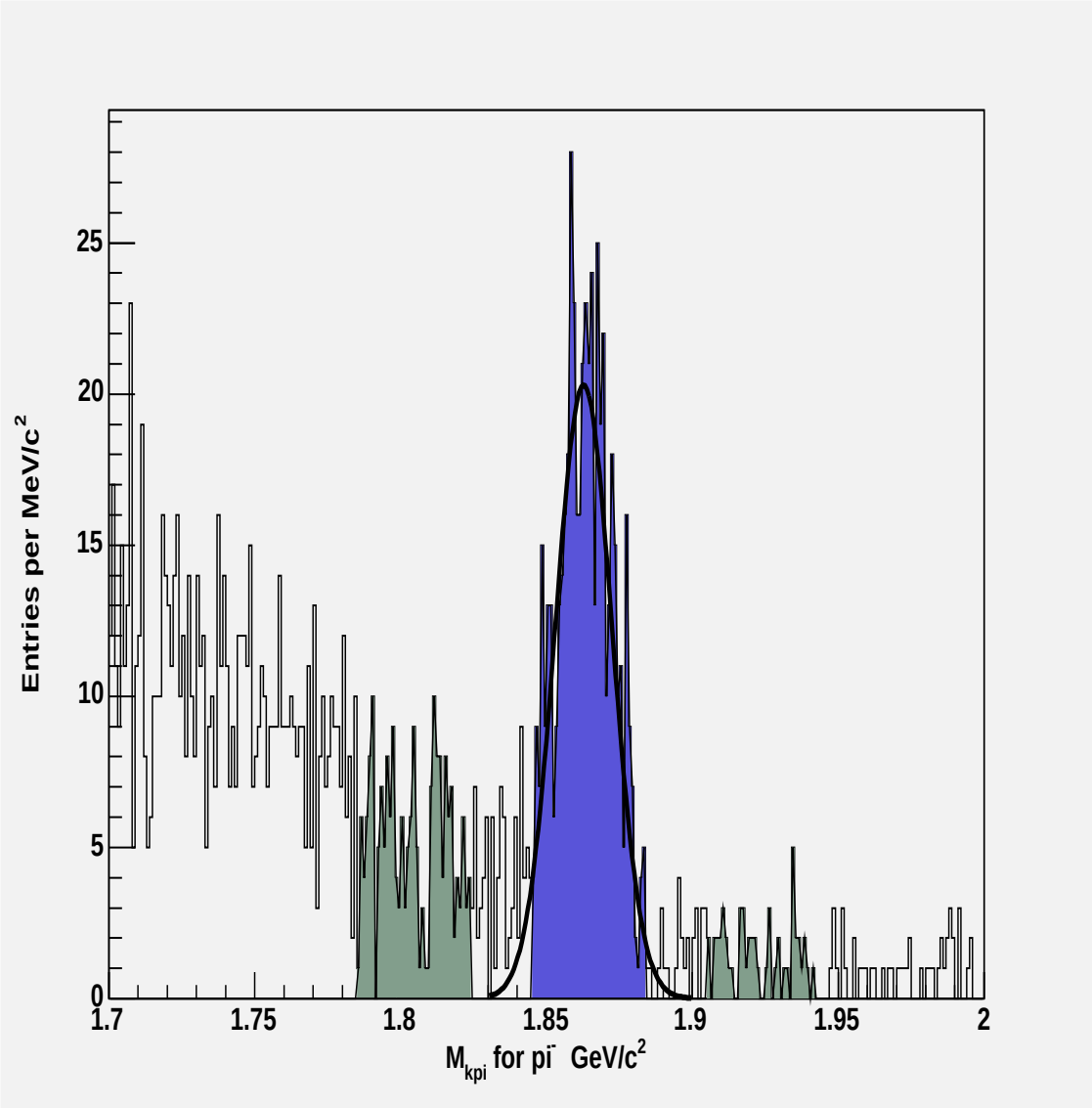

Figure 4.10: The mass distribution spectrum for the π^- particle with the electron likelihood in $D^0 \rightarrow K\pi$ decay. Gaussian signal over the range 1.83 GeV/c^2 to 1.90 GeV/c^2 is fit over the signal peak. The mass window for the signal peak lies between 1.845 GeV/c^2 - 1.885 GeV/c^2.The lighter shaded regions on both sides of signal peak are the sidebands used to estimate the background.

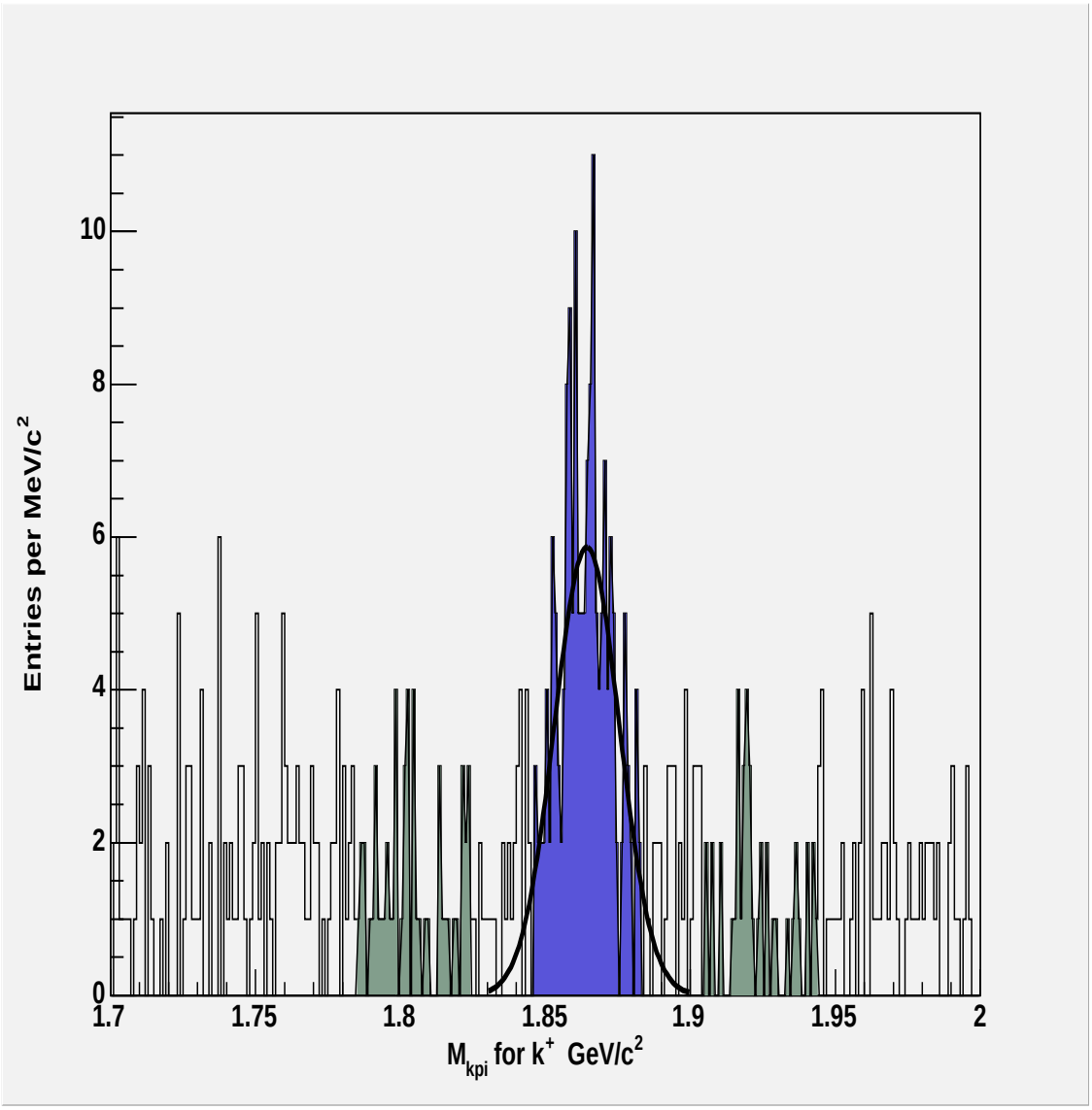

Figure 4.11: The mass distribution spectrum for the K^+ particle with the electron likelihood in $D^0 \rightarrow \mathrm{K}\pi$ decay. Gaussian signal over the range 1.83 GeV/c^2 to 1.90 GeV/c^2 isfit over the signal peak. The mass window for the signal peak liesbetween 1.845 GeV/c^2 - 1.885 GeV/c^2.The lighter shaded regions on both sides of signal peak are the sidebands used to estimate the-background.

Chapter 5

Conclusions

We report on the preliminary investigation of the search for the flavor changing neutral current decay $D^0 \rightarrow e^+e^-$ in $p\overline{p}$ collisions at $\sqrt{s} = 2.0$ TeV using data collected by CDF II at the Fermilab Tevatron Collider. From Monte Carlo simulation of $D^0 \rightarrow e^+e^-$ and $D^0 \rightarrow K\pi$ decays, we find the efficiency and acceptance ratios. The number of reconstructed candidates from simulation is 7328 (Kπ) and 1869 (ee) for the two decay modes with a ± 20 MeV/c^2 signal window, yielding a product of acceptance and efficiency to be $3.42 \pm 0.05\%$. As the mass window for $D^0 \rightarrow e^+e^-$ decay is opened more, the acceptance ratio increases to 10 %.

The decay chain for $D^{*+} \rightarrow D^0$ ($\mathrm{K}^-\pi^+$) π_s^+ and charge conjugate, is reconstructed using dataset h77jc0 and used to determine the electron fake rates for the $\pi's$ and $K's$ from the D^0 decay. The number of candidates under the signal peak and the sidebands are found from plots of the D^0 and $\overline{D^0}$

candidate mass distributions, with and without requiring tracks to satisfy the electron likelihood requirement $\mathcal{L} > 0.9$ and are used to calculate the electron fake rates for the D^0 daughter particles. The measured values for K^+, K^-, π^+, π^- are $(5.59 \pm 0.50) \times 10^{-4}$, $(4.96 \pm 0.98) \times 10^{-4}$, $(2.27 \pm 0.39) \times 10^{-3}$ and $(1.66 \pm 0.46) \times 10^{-3}$ respectively. The electron fake rate determination can be improved by running the process on a larger data sample, and finding the fake rates as a function of track p_T. But, these low values imply that the backgrounds to $D^0 \rightarrow e^+e^-$ should be quite small, and that we should be able to make an estimate of the sensitivity.

To find the sensitivity for the branching ratio of $D^0 \rightarrow e^+e^-$ events, we use Eq. (1.1). The number of events N(Kπ) from the $360pb^-$ dataset is about 10^6. At 90% confidence level, assuming no observed signal or background, the upper limit on the number of D$^0 \rightarrow e^+e^-$ events is $N(e^+e^-) \leq 2.3$. The $\mathcal{B}$ ($D^0 \rightarrow$ Kπ) is 3.80 %. The upper limit on the branching fraction of $\mathcal{B}$ ($D^0 \rightarrow e^+e^-$) at 90% confidence level would then be: $\mathcal{B}(D^0 \rightarrow e^+e^-) \leq 2.9 \times 10^{-6}$. The current best experimental limit is 1.2×10^{-6}.

We can improve the sensitivity for the branching fraction by using a larger data sample. Also the efficiency and acceptance ratios may be improved if electron tracks are corrected for energy loss.

Appendix A

Selection files and C++ code used in analysis

The decay table used for the selection of $D^0 \rightarrow e^+e^-$ is :

```
------------------
# Decay D0 1.0000   e+ e-                              PHSP;
 Enddecay
Decay K*0R 1.0000   K0 pi0                               VSS;
 Enddecay
Decay anti-D0 1.0000   e+ e- PHSP;
Enddecay

 Decay D_s+ 0.0200
phi   e+     nu_e       PHOTOS ISGW2;
```

```
 0.0260    eta   e+ nu_e PHOTOS ISGW2;
-------------------
```

The decay table used for the selection of $D^0 \to K\pi$ decay is:

```
-----------------------
 Decay K*BR 1.0000   anti-K0  pi0                          VSS;
Enddecay
 Decay D0 1.0000   K-  pi+                            PHSP;
Enddecay
  Decay K*0R 1.0000   K0 pi0 VSS;
 Enddecay
 Decay anti-D0 1.0000   K+  pi- PHSP;
  Enddecay
    Decay D_s+ 0.0200    phi e+     nu_e       PHOTOS ISGW2;
-------------------------
```

To make BStntuples, CandsExe is run on the Monte Carlo events. Candsfitter module collects D* tagged D^0 particles decaying into Kπ and to ee decay mode:

```
#-------------------------------
 # D0 In simplest topology only
#-------------------------------
```

```
#Use CandsFitter here because we already have the 2Pi coll
 module clone   CandsFitter D-KPi
module enable  CandsFitter-D-KPi module talk    CandsFitter-D-KPi
  source $env(ENV_TCL_DIR)/trigTwo.tcl
  Cuts
    verbose     set 0
    reject      set 0
    massMin     set 1.500
    massMax     set 2.000
    chi2Max     set 15
    deltaZ0Max  set 1.5
  exit
  CandsFitter-D-KPi
    iDCollDesc  set All-2Pi
    oDCollDesc  set D-KPi
    pid         set 421
    iSCollDesc  set All-Kaons
    nReplace    set 1
    chargeP12   set -1
  exit
exit
  --------------------
```

Further analysis is done on the BStntuple so formed which writes the output in a root file. Selection cuts can be made on this root file:

```
#define DstarAna_cxx #include "DstarAna1.h" #include "TH2.h"
#include "TH1.h" #include "TStyle.h" #include "TCanvas.h" void
DstarAna::Loop() {
   if (fChain == 0) return;
   Int_t nentries = Int_t(fChain->GetEntriesFast());
   Int_t nbytes = 0, nb = 0;
   hfile = new TFile("tree14b3.root","RECREATE","histograms");
   cout << "created tree14b3.root."<<endl;
   //Book Histograms
   const Int_t npart = 4 ;// 4 types of particles: K +/- and pi +/-
   const char* part[] = {"K-","pi+","pi-","K+"};
  ----------------------
          hmass[i][j] =  new TH1F(hid, title, 200, 1.60,2.0);
   ---------------------
      if((DKLxyz>0)&&(Dchisq<9)){
      if (((KAONPt>2.0)&&(KAONPt<15.0))&&(PIONTPt>2.0)&&(PIONTPt<15.0))){
      if(qpionPt>0){
                  h = hmass[0][0];
               h->Fill(MDkpi);
              if(likelihoodk>0.9){
                h = hmass[0][1];
```

```
----------------------
 Float_t N1,N2,N3,Nav;
 for (Int_t i = 0; i<npart; i++){
  for (Int_t j=0; j<neid; j++){
    h=hmass[i][j];
 ----------------------
    N3= h ->Integral(146,166);


    hfile->Write();
 ------------------------
```

Appendix B

Runlist for Monte Carlo simulation

The Run2 offline system is used for the data processing.The following instructions at the time of login define the environment variables and path for the analysis.The version used for my Monte Carlo simulation is 5.3.4 which processes data on the production farm.

```
source ~cdfsoft/cdf2.cshrc
setenv USESHLIBS 1
setup cdfsoft2 5.3.4
```

The runlist used for my analysis contains runs from 138809 to 186598.This runlist contains 115 runs covering 25% of the total luminosity.This is subdivided into 25 intervals each having 4 Pb^{-1} luminosity. All runs have SVT beamline information. Instructions to run B-Physics Monte Carlo are fol-

lowed to generate events.The executables for this are pre-compiled. The parameters for the random number generation, specific decay, run numbers to be used, trigger type etc are all mentioned in the makeplan.pl script. The tcl templates for Simulation and Trigger Simulation are included here. Enabling shared libraries debugs and tests code faster.

Bibliography

[1] S. Gasiorowicz and P. Langacker, "Elementary Particles in Physics", in Encyclopedia of Physics, Third Edition, Wiley-VCH(2005).

[2] D.E. Groom *et al.*, "Particle Data Group", Eur. Phys. Jour. C15, 1 (2005).

[3] B R. Martin and G. Shaw,"Particle Physics", 2nd Edition, John Wiley & Sons Ltd., ISBN: 0-471-97252-5(1997).

[4] Donald H. Perkins, "Introduction to High Energy Physic",Third Edition, Addison-Wesley Publishing Company Inc., ISBN 0-201-12105-0(1986).

[5] Gustavo Burdman, Eugene Golowich, JoAnne Hewett ,and Sandip Pakvasa, "Rare charm decays in the standard model and beyond", Phys. Rev. D66,014009(2002).

[6] B. Aubert, *et. al*, "Search for Flavor-Changing Neutral Current and Lepton-Flavor Violating Decays of D0$\rightarrow l^+l^-$", Phys.Rev.Lett. 93,191801(2004).

[7] Sandip Pakvasa, "Flavor Changing Neutral Currents in Charm sector", UH-511-871-97(1997).

[8] A. Freyberger *et al*, "Limits on Flavor Changing Neutral Currents in D0 Meson decay", Phys. Rev. Lett. 76, 3065-3069(1996).

[9] D. Spelbring *et al*, "Search for D0(1865) mesons produced in association with prompt muons in hadronic interactions", Phys. Rev. Lett. 40, 605-607(1978).

[10] Bill Ashmanskas, Rob Harr, "Search for the FCNC decay D0$\rightarrow\mu^+\mu^-$", CDF/ANAL/BOTTOM/CDFR/6273(2003).

[11] Chunhui Chen, Ph.D. Dissertation, Univ. of Pennsylvania(2003).

[12] A. Bardi *et al.*, "The CDF-II online Sillicon Vertex Tracker", Presented at 8th International Conference on accelerators and Large Experimental physics control systems, San Jose,California, arXiv.org/hep-ph/0112141(2001).

[13] Gino Bolla, "Status of the CDF Silicon Detector", Eur.Phys.Jour.C 33,(2004).

[14] Y. fukui, M. Mishina *et.al*, "CDF End plug Electromagnetic Calorimeter.Using Conductive plastic proportional tubes", FERMILAB-PUB-87/173-E.

[15] William F. Badgett,Jr., "Design, Performance and Control of the CDF Run 2 Data Acquisition System", IEEE Nuclear Science Symposium(2004).

[16] E. Gerchtein , M. Paulini, "CDF Detector Simulation Framework and Performance", arXiv.org/abs/physics/0306031(2005).

[17] Ken Bloom, "Getting Started with CDF Run 2 Offline", CDF/DOC/COMP_UPG/CDFR/5294, Version 4.7.1.

[18] M. Casarsa, A. Fella, Y. Gotra, R. Kennedy, T. Kim, M. Neubauer, F. Semeria, I. Sfiligoi, A. Sidoti, F. Wurthewein. " CDF CAF User's M anual", Version 1.0, March 2005, CDF/DOC/COMP_UPG/PUBLIC/6092.

[19] www−cdf.fnal.gov/upgrades/computing/offlinehowto/HowtoGenSim.html

[20] R. Culbertson *et al*, "Stntuple Manual", http://fcdfwww.fnal.gov/∼cdfopr/Stntuple/Stntuple.pdf, Version 1.01, Nov.2005.

[21] V. Tiwari, G. giurgiu, M. Paulini ,and J. Russ, "Likelihood based electron tagging", CDF/ANAL/BOTTOM/CDFR/7121, Version 1.3(2004).

[22] E.Berry, D.Dhaliwal, I.K. Furić, R. Harr, Y.K.Kim, Ch. Paus, T. Spears, "Study of Muon Matching Efficiencies and Mistag rates", CDF/DOC/BOTTOM/CDFR/8042, Version 1.0(January 2006).

[23] D. Acosta *et al*, "Search for the Flavor-Changing Neutral Current Decay D0$\rightarrow\mu^+\mu^-$ in p$\bar{p}$ Collisions at $\sqrt{s}$=1.96 TeV", arXiv.org/hep-ex/0308059.

[24] P.L. Frabetti *et al*, "Search for CP Violation in Charm Meson Decay", Phy. Rev. D50, R2953-R2956(1994).

[25] D. Acosta *et al*, "Search for $B_s^0 \to \mu^+\mu^-$ and $B_d^0 \to \mu^+\mu^-$ Decays in p$\bar{p}$ Collisions at $\sqrt{s}$=1.96 TeV", Phys. Rev. Lett. 10,1103 93-03(2001).

[26] D0 Collaboration: V.M. Abazov, *et al*, "A Search for the Flavour-Changing Neutral Current Decay $B_s^0 \to \mu^+\mu^-$ in p$\bar{p}$ Collisions at $\sqrt{s}$=1.96 TeV with the D0 detector", Phys. Rev. Lett.94, 071802(2005).

[27] J.L. Hewett, "Searching for new Physics with charm", SLAC-PUB-95-6821(1995).

[28] Gustavo Burdman, Eugene Golowich, JoAnne L. Hewett, and Sandip Pakvasa, "Radiative weak decays of charm mesons", Phys.Rev.D.52,6383-6399(1995).

[29] Zhibin Huang, Ph.D. Dissertation, Wayne State University(2003).

[30] Julia Thom, "Rare charm and B decays at CDF", Eur. Phys. Jour. C33(2004).

[31] E.M. Aitala *et al*, "Search for CP violation in charged D meson decays", Phys. Lett. B403,377-382(1997).

[32] R.M. Baltrusaitis *et al*, "Measurements of Cabbibo-Suppressed Hadronic decays of charmed D+ and D0 mesons", Phys. Rev. Lett. 56, 2140(1986).

[33] D. J. Summers *et al*, "Search for rare and forbidden charm meson decays at fermilab" E791, UMS/HEP/2000-030; FERMILAB-conf-00/223-E.

abstract

resume